

*To be published in "Computational Modeling of Membrane Bilayers" (ed. Scott E. Feller),
Current Topics in Membranes, vol. 60, Elsevier*

Considerations for Lipid Force Field Development

Jeffery B. Klauda, Richard M. Venable, and Richard W. Pastor
klauda@helix.nih.gov, venabler@nhlbi.nih.gov, pastorr@nhlbi.nih.gov

Laboratory of Computational Biology, National Heart, Lung, and Blood Institute,
National Institutes of Health, Bethesda, MD 20892, USA

Alexander D. MacKerell, Jr.
alex@outerbanks.umaryland.edu

Department of Pharmaceutical Sciences, School of Pharmacy, University of Maryland,
Baltimore, MD, 21201, USA

Abstract

The underlying approach to development of the CHARMM lipid force field, and the current *ab initio* and molecular dynamics methods for optimization of each term are reviewed. Results from the recent revision of the alkane force field and new results for esters illustrate the dependence of torsional surfaces on level of theory and basis set, and how changes in the surface manifest themselves in alkanes and dipalmitoylphosphatidylcholine (DPPC) bilayers. The following properties from simulation and experiment on DPPC bilayers are compared: structure factors from x-ray diffraction; deuterium order parameters; NMR spin lattice relaxation times; lipid translational diffusion constants; elastic moduli; and the dipole potential. The importance of including long-range Lennard-Jones interactions and taking finite system size into account is stressed. Theoretical and practical aspects associated with surface tensions and surface areas of lipid bilayers and monolayers are discussed.

I. Introduction

Papers describing simulations of lipid bilayers emerged in earnest in the late 1980's and early 1990's, and many included the phrase "the field is in its infancy". This fairly harmless phrase promises high potential, and requests understanding for results that are not immediately useful. Additionally, it implies the need for substantial care and feeding.

A critical component of the care and feeding has been the development of a reliable force field (FF) or potential energy function. A simulation can't proceed without it, and the availability of the appropriate FF is among the first issues that a simulator must confront when considering a new system. This chapter describes the approach taken in the development of the recent CHARMM (Chemistry at HARvard Macromolecular Mechanics) (Brooks et al., 1983) all-atom lipid force fields, including the set currently under development. This approach consists of two basic steps: (1) optimization of terms in the empirical energy function using quantum mechanical (QM) calculations, molecular dynamics (MD) simulations, and experimental data on appropriate small molecules; (2) MD simulations of lipid bilayers and monolayers, and comparison with target data. This process directly links the behavior of the large assembly to the underlying physics of its components, and thereby lends confidence that agreement with experiment is not fortuitous. To provide a specific example, the recent dihedral parameters for the acyl chain of lipids in C27r (Klauda et al., 2005a) were generated by high level *ab initio* calculations on butane through heptane. MD simulations were then carried out on liquid heptane, decane, tridecane, and pentadecane, to confirm that C27r yielded better agreement with experiment than the previous set, C27 (Feller and MacKerell, 2000). Then simulations on a dipalmitoylphosphatidylcholine (DPPC) bilayer were carried out, and the results were compared with experimental deuterium order parameters, x-ray diffraction density profiles, and conformational populations from infrared spectroscopy.

The core of this chapter is contained in the following two sections. Section II describes the optimization of the FF for small molecules; *i.e.*, step one of the process just outlined. The section begins with a review of *ab initio* calculations to provide a sense of the level of theory and system size accessible with presently available computers, and the specific choices used in CHARMM parameterization. Sections II.B.1 and II.B.2 detail

the optimization of the electrostatic and Lennard-Jones terms, respectively. Section II.B.3 considers the torsional terms, and includes *ab initio* results for the torsional surfaces of alkanes and esters to illustrate the effects of level of theory and implicit solvation. Lastly, Section II.C reviews the assessment of C27 and C27r from MD simulations of liquid alkanes in the bulk and the interface.

Section III describes seven classes of membrane target data that are presently being used in testing of CHARMM parameter sets. These are: (A) structure factors from x-ray diffraction; (B) deuterium order parameters; (C) NMR spin lattice relaxation times; (D) translational diffusion constants; (E) elastic moduli; (F) surface areas and surface tensions of bilayers and monolayers; (G) and the dipole potential. Each topic is paired with a technical nuance (*e.g.*, finite size effects and translational diffusion), and the ordering is roughly from better to worse in terms of agreement of simulation and experiment or in ease of interpretation. As for Section II, the results of C27 and C27r are compared. The reader primarily interested in the performance of CHARMM for membranes may consider reading Section III before Section II.

Section IV summarizes the results, and considers some of the broader questions of parameter development. The remainder of this introductory section defines the terms of the CHARMM FF.

The potential energy $V(\hat{R})$ in the CHARMM FF (MacKerell, 2004) is a function of the positions of all of the atoms in the system. Like most FF used for MD simulations of macromolecules and membranes, it has the following general form:

$$\begin{aligned}
 V(\hat{R}) = & \sum_{bonds} K_b (b - b_0)^2 + \sum_{angles} K_\theta (\theta - \theta_0)^2 + \sum_{dihedrals} \left[\sum_j K_{\varphi,j} (1 + \cos(n_j \varphi - \delta_j)) \right] \\
 & + \sum_{\substack{nonbonded \\ pairs\ i,j}} \varepsilon_{ij} \left[\left(\frac{R_{min,ij}}{r_{ij}} \right)^{12} - \left(\frac{R_{min,ij}}{r_{ij}} \right)^6 \right] + \sum_{\substack{nonbonded \\ pairs\ i,j}} \frac{q_i q_j}{\varepsilon_D r_{ij}}
 \end{aligned}
 \tag{1}$$

The first three terms parameterize the interactions of atoms chemically bonded to each other, and are referred to as the *intramolecular* or *internal* terms. The last two (commonly referred to as the *nonbond*, *intermolecular*, or *external* terms) describe the van der Waals and electrostatic interactions between atoms, respectively. More

specifically, bond stretches and bends are harmonic, with force constants K_b and K_θ , and equilibrium values b_0 and θ_0 . While more complex functional forms, such as the Urey-Bradley and improper dihedrals, are available in CHARMM, they are only used for a subset of the functionalities in lipids. Dihedral, or torsion, angles are parameterized by a cosine series where K_φ , n and δ are the force constant, multiplicity and offset, respectively. Lipid torsions are described by sets of $K_{\varphi,j}$, n_j and δ_j , where j can range from 1 to 6. Explicit coupling between neighboring torsions, which is important for proteins and peptides is described by the “CMAP” correction (Buck et al., 2006; MacKerell et al., 2004) has not been introduced to the lipid FF. Van der Waals interactions are treated by the well-known Lennard-Jones (LJ) “6-12” potential, where ϵ_{ij} is the potential energy minimum between two particles, and $R_{\min,ij}$ is the position of this minimum. Given that the repulsive wall is multiexponential, that the attractive interaction is more accurately described as the asymptotic series $\sum_{n=3}^{\infty} r^{-2n}$, and that chemically similar (but not identical) atoms share the same LJ parameters, this part of the FF contains more uncertainty than the preceding bonded terms. It is, accordingly, the most difficult to parameterize. Lastly, q_i and q_j are the atomic partial charges, and ϵ_D is the dielectric constant. The membrane systems considered here include all lipids and water, so $\epsilon_D=1$. C27 and C27r are “additive models”. That is to say, the partial charges are fixed throughout the simulation, and the electrostatic energy is the sum of 2-body terms. Polarizable models allow the partial charges to vary in response to their environment (the interactions are non-additive, or multibody), and provide a more accurate, though computationally more demanding, description of the system. There is not presently a polarizable lipid FF in CHARMM, though classical Drude based models (Rick and Stuart, 2002) for water (Lamoureux et al., 2003), alkanes (Vorobyov et al., 2005), and ethers (Vorobyov et al., 2007) have been developed. Efforts to develop a polarizable lipid model compatible with the fluctuating charge protein model implemented in CHARMM (Patel et al., 2004) are also ongoing.

The basic form of Eq. (1) is utilized for all classes of molecules in CHARMM, including proteins, DNA, carbohydrates and ethers, and these sets are all designed to be

compatible (*e.g.*, a peptide to be simulated in a membrane environment does not require new parameters). Hydrogens are explicitly included to retain consistency with the other classes of molecules, and because they were found to be necessary for describing the more condensed crystal and gel phases of lipid bilayers (Venable et al., 2000).

Section II. Quantum Mechanics and Molecular Dynamics Based Parameter Optimization

A. Overview of quantum mechanical methods

As emphasized in Section I, an essential component in the parameterization the CHARMM FF is quantum mechanics. Ideally, QM calculations would be carried out on a sufficiently large cluster of molecules to include all of the essential interactions necessary for parameterizing the molecular mechanics potential energy function given by Eq. (1). For lipids in a bilayer, one might imagine that such cluster would consist of three lipids and 10 hydrating waters/lipid. DPPC (Fig. 1) contains 50 heavy atoms, so the preceding hypothetical cluster contains 180 heavy atoms. This is well outside the range of 10-12 heavy atoms that can presently be evaluated accurately with the high-level *ab initio* calculations that force field parameterizations require. In addition, limitations in low-level QM calculations with respect to London's dispersion interactions for small clusters of molecules hinder the use of QM data alone in parameter optimization (MacKerell, 2004). To understand why, requires a brief review of the approximations to the exact time-independent Schrödinger equation:

$$\mathcal{H}|\Psi\rangle = \mathcal{E}|\Psi\rangle \quad (2)$$

where \mathcal{H} is the Hamiltonian operator for the system of nuclei and electrons, $|\Psi\rangle$ is the electron wave function, and \mathcal{E} is the energy (Szabo and Ostlund, 1996). Even after the nuclear and electron energies are separated by applying the Born-Oppenheimer approximation, Eq. (2) can, in general, be solved analytically only for one-electron systems (this is similar to the many-body problem in classical simulations). Numerical solutions for the exact Hamiltonian are possible for more than one electron, but for the applications considered here further simplifications are required. These are divided into

simplifications to \mathcal{H} (*level of theory*) and to $|\Psi\rangle$ (*basis set*). At the exact level of theory, denoted full configuration interaction (CI), all electrons interact with each other. The basis set defines the range of spatial coverage and spin for each electron. An exact solution to Eq. (2) requires an infinite basis set, which may be asymptotically approximated using a complete basis set (CBS) extrapolation (Dunning, 2000). More basis functions result in greater accuracy in the eigenvalue, \mathcal{E} . Hence, both electron correlation and completeness of a basis set must be considered when calculating interaction and conformational energies from QM to develop an accurate force field.

The simplest *ab initio* (as apposed to semi-empirical) approximation to \mathcal{H} is that of Hartree and Fock (HF). Here the energy is iteratively minimized by altering the occupation of the spin orbitals using an effective one-electron operator, *i.e.*, an electron interacts with an average potential of the surrounding electrons. This replaces the many-electron problem in Eq. (2) with many one-electron problems. However, HF is in many cases a poor approximation to the Hamiltonian, and, by itself, is often inadequate for parameterization studies. For example, the attractive energy between two ideal gas atoms arises from electron correlation (induced dipole-induced dipole interactions and similar higher order terms). HF yields only repulsive energies because electron correlation is absent.

The electron correlation energy is defined as the additional energy beyond the HF limit (HF energy with an infinitely-sized basis set) due to explicit electron-electron interactions. Many methods have been developed to include electron correlation. Density functional theory (DFT) is the simplest and the least computationally demanding. Examples include commonly used B3LYP (Becke, 1993) and PBE (Ernzerhof and Scuseria, 1999) functionals. However, DFT methods lack the ability to accurately describe the long-range dispersion interactions important for lipid model molecules. Second order Møller-Plesset perturbation theory (MP2) is the most efficient method that includes electron correlation and dispersion interactions (Dunning, 2000). This method incorporates a perturbation in the HF Hamiltonian, \mathcal{H}_0 ,

$$\mathcal{H}|\Psi\rangle = (\mathcal{H}_0 + \mathcal{V})|\Psi\rangle = \mathcal{E}|\Psi\rangle \quad (3)$$

where \mathcal{V} is the perturbation of \mathcal{H}_0 from the true \mathcal{H} . The exact eigenfunctions and eigenvalues are expanded in a Taylor series where the second order term in the expansion is the additional energy in MP2 beyond the HF value. The coupled cluster method, CCSD(T), (Raghavachari et al., 1989) is the most accurate of these commonly used correlative methods and typically approaches the full CI result (Dunning, 2000).

Just as the level of theory is important in calculating energies from QM, so too is the size of basis sets used to represent the wave function. Basis sets typically consist of Gaussian-based functions that represent orbitals, such as s, p, d and f. The correlation consistent basis sets by Dunning et al. (2001) have been optimized for consistent convergence of energy for correlated methods and are typically used with these abovementioned approximations of \mathcal{H} . In the development of the dihedral portion of the CHARMM force field, the following basis sets are used in increasing order of complexity: cc-PV n Z where n can be D (double), T (triple), Q (quadruple), and 5 (quintuple). The computational time required for DFT, MP2, and CCSD(T) typically scales with the number of basis functions to the power of 2.5, 3.5, and 6, respectively. Consequently, these methods are especially limited by the number of basis functions or equivalently the number of electrons.

Computations at CCSD(T) with a large basis set such as cc-PV5Z (denoted CCSD(T)/cc-PV5Z), would result in accurate energies for most compounds. However, this is currently too computationally demanding for a system with more than three or four heavy atoms. QM hybrid methods have been developed to increase the system size based on the approximation that electron correlation and basis sets are additive. The G3 method is an example (Curtiss et al., 1998; Curtiss et al., 1999). It combines high-level energy calculations (*e.g.*, CCSD(T)) with small basis sets, and lower level calculations (MP2 and MP4) with larger basis sets. The G3 method results in accurate heats of formation, ionization potentials, electron affinities, and proton affinities. Kluda et al. (2004) developed a similar method referred to as HM-IE (the **H**ybrid **M**ethod for **I**nteraction **E**nergies) that accurately approximates the interaction energy calculated with CCSD(T) and a large basis set but uses considerably less computational time and resources. This method was developed for intermolecular energies but can also be used for intramolecular conformational energies,

$$\begin{aligned}
E[\text{CCSD(T)/LBS}] &= E[\text{CCSD(T)/SBS}] \\
&\quad + (E[\text{CCSD(T)/LBS}] - E[\text{CCSD(T)/SBS}]) \\
&\equiv E[\text{CCSD(T)/SBS}] + (E[\text{MP2/LBS}] - E[\text{MP2/SBS}]) \quad (4) \\
&\equiv E[\text{MP2 : CC}]
\end{aligned}$$

where SBS denotes the small basis set and LBS denotes the large basis set. For MP2:CC, the basis set contribution going from the CCSD(T)/SBS to CCSD(T)/LBS is approximated by the difference between the interaction energies at MP2 with the same two basis sets. Only two sets of energy calculations are required in Eq. (4), and these are calculated in the following order: (1) CCSD(T)/SBS, which includes the MP2/SBS calculations since CCSD(T) uses the MP2 result; and (2) MP2/LBS.

B. Parameterization of force fields

In principle, the same set of QM calculations could be used to parameterize each portion of the force field. In practice, the different terms of Eq. (1) are computed independently. There are a number of reasons for this approach. As already noted, the fragments that can presently be treated with highly accurate QM methods are relatively small, 10-12 heavy atoms, and the optimal systems for evaluating each type of interaction differ. The level of theory, basis set, and adjustments for solvent effect appropriate for these systems also differ. Finally, the approach also allows incremental, yet important improvements. For example, C27r was developed leaving all non-bonded terms and the head group torsions unchanged; *i.e.*, only the torsional potential of the acyl chains was modified.

The nonbonded terms are evaluated first for the given atom types and are described in the following two subsections. Since these are primarily parameterized for intermolecular interactions, adjustments are needed for the short-range intramolecular interactions that impact the conformational properties of a molecule via the dihedral potential. These changes are especially important for obtaining the proper secondary structure of proteins (Duan et al., 2003; Feig et al., 2003; Jorgensen et al., 1996; MacKerell et al., 1998) and conformations of dihedral states in lipids (Klauda et al., 2005a). The QM methods used to parameterize the dihedral potential are discussed in subsection B.3.

B.1 CHARMM electrostatic potential terms.

Optimization of the electrostatic terms (the partial atomic charges q_i in Eq. (1)) is mostly based on QM data. Charges in most current empirical force fields are assigned either by fitting to QM electrostatic potential (ESP) maps (Bayly et al., 1993; Chirlian and Francl, 1987; Henchman and Essex, 1999; Merz, 1992; Singh and Kollman, 1984), or by the supramolecule approach (MacKerell, 2004). Charge determination via ESP fitting involves adjustment of the partial atomic charges to minimize the RMS difference between the QM and empirical ESP maps. This approach may be used to rapidly obtain charges for a wide range of molecules, although the charges are representative of the gas phase and may be sensitive to conformation; these issues have been addressed in different contexts (Bush et al., 1999; Jakalian et al., 2000; Laio et al., 2002). In the supramolecule approach, which is used in the CHARMM and the OPLS force fields (Jorgensen et al., 1996), the partial atomic charges are adjusted to reproduce QM minimum interaction energies and geometries of model compounds with water or for model compound dimers; dipole moments from either QM or experiment may also be included as target data. This approach allows for local polarization associated with the interaction between the molecules to be included in the fitting, and for further optimization based on experimental data for model compound pure solvents and their free energies of solvation (Oostenbrink et al., 2004; Vorobyov et al., 2007). The level of theory used in determination of the intermolecular interactions in CHARMM additive FF is HF/6-31G*. While there are limitations with HF level calculations, its selection is partly based on historical reasons: its initial application to CHARMM parameterization in the 1980's was aimed at hydrogen bond interactions; these are dominated by electrostatic interactions, which are satisfactorily treated at the HF level. HF/6-31G* also tends to overestimate dipole moments, and thereby mimics the overpolarization that occurs in condensed phases. In addition, for polar, neutral compounds in CHARMM, the QM interaction energies are scaled by 1.16 prior to their use as target data to account for limitation in the level of theory, the required overpolarization that occurs in the condensed phase and many-body effects. These effects are also accounted for by offsetting the QM minimum interaction energy distances by 0.1 to 0.2 Å (*i.e.*, the empirical distances should be shorter than the QM distances by that amount), which is important for reproducing the

correct experimental densities. While the above approach includes a variety of assumptions and higher QM levels of theory are certainly accessible, when optimizing charges for new molecules for use with the CHARMM additive force field the same approach should be used to maintain consistency.

Inherent in the supramolecule approach to charge optimization is the water model. This is because the overall parameter set must balance solvent-solvent, solvent-solute and solute-solute interactions (the so called interaction triad). The TIP3P model (Jorgensen et al., 1983) is the standard in CHARMM. In this model the dipole moment is overestimated as required to yield the proper pure solvent properties. This overestimation leads to a water dimer interaction energy that is significantly too favorable, and this must be taken into account when adjusting the partial atomic charges of model compounds. Consequently, once chosen, a water model cannot be easily replaced. It is strongly suggested that the TIP3P model, despite its deficiencies, be used in simulations with the CHARMM lipid force field.

B.2 CHARMM Lennard-Jones potential terms

The LJ parameters are both critically important and very difficult to optimize. Their importance is based on their significant contribution to pure solvent properties (MacKerell and Karplus, 1991) and the difficulty is, in part, due to the current inability of QM methods to adequately treat dispersion interactions for large systems. For example, the use of QM data on small clusters to optimize the LJ parameters leads to poor condensed phase properties. This requires that the optimization of LJ parameters be performed by empirical fitting to reproduce thermodynamics properties from condensed phase simulations, generally of neat liquids (Jorgensen, 1986; Jorgensen et al., 1984). Properties targeted include heats of vaporization, densities, isothermal compressibilities, and heat capacities. Alternatively, heats or free energies of aqueous solvation, partial molar volumes or heats of sublimation and lattice geometries of crystals can be used as the target data (MacKerell et al., 1995; Warshel and Lifson, 1970). This approach has been applied extensively in the development of the CHARMM lipid force field (Feller and MacKerell, 2000; Feller et al., 1997b; Schlenkrich et al., 1996; Vorobyov et al., 2007). However, reliance on condensed phase data alone leaves the LJ parameters underdetermined (MacKerell, 2001). This problem has been overcome by determining

the relative values of the LJ parameters via high-level QM data of interactions of the model compounds with rare gases (Yin and MacKerell, 1996) while the absolute values are based on the reproduction of experimental data (Chen et al., 2002; Yin and MacKerell, 1998). This approach is tedious as it requires supramolecular interactions involving rare gases; however, once satisfactory LJ parameters are optimized for atoms in a class of functional groups they typically can be directly transferred to other molecules with those functional groups without further optimization.

An extensive set of nonbond parameters for the CHARMM force fields has been produced using the above approaches. These parameters are correlated, and it is essential that modifications be introduced consistently, and with the water model taken into account. For example, if the partial charges for a model are changed then it is necessary to reoptimize the LJ parameters to maintain the agreement with condensed phase properties. Alternatively, alteration of either the charges or LJ parameters typically requires reoptimization of the dihedral parameters. Additional information on parameter optimization may be found elsewhere (MacKerell, 2001; MacKerell, 2004; MacKerell, 2005), including the web page of Prof. MacKerell (MacKerell, 2007).

B.3 CHARMM dihedral potential terms

This subsection presents a description of specific QM methods used to parameterize the aliphatic and glycerol portion of the CHARMM lipid FF for DPPC. In keeping with the size limitations of accurate *ab initio* calculations, the first step of the parameterization involves choosing appropriate model compounds. Here the aliphatic portion of DPPC is modeled as heptane (Fig. 1b), and the linking region of the aliphatic chains with the glycerol is modeled by isopropyl butyrate (a branched ester, Fig. 1c) for chain 2, and *n*-propyl butyrate (a linear ester, Fig. 1d) for chain 1.

Conformational energies are evaluated from minimum energy geometries. The levels of theory and basis sets, however, need not be the same for geometry optimization and energy evaluation. The MP2 level of theory is usually sufficient for predicting the *structure* of ground state molecules. Since the computational time scales with the number of basis functions, optimization with the small yet accurate basis sets is preferred. A series of geometry optimizations with multiple basis sets is required to justify the

accuracy of the methods. For pentane, the calculated MP2/cc-pVTZ energy difference from all-*trans* conformer (*tt*) and the *trans-gauche* (*tg*) conformer optimized with MP2/cc-pVDZ and MP2/6-311++G** is 0.558 and 0.553 kcal/mol, respectively (Klauda et al., 2005a). The difference between the optimized structure at a double- ζ basis set (cc-pVDZ) and a triple- ζ basis set (6-311++G**) is small and geometries of all the alkanes were optimized with MP2/cc-pVDZ. Similarly, there is little basis set dependence of the β_4 torsion energy profile for isopropyl butyrate (Fig. 2). Only at $\beta_4=120^\circ$ are the MP2/cc-pVTZ//MP2/cc-pVTZ energies slightly lower than MP2/cc-pVDZ//MP2/cc-pVTZ. The preceding results imply that MP2/cc-pVDZ optimizations are accurate for short alkanes and the two esters. However, this should not be assumed for other small molecules without similar testing procedures.

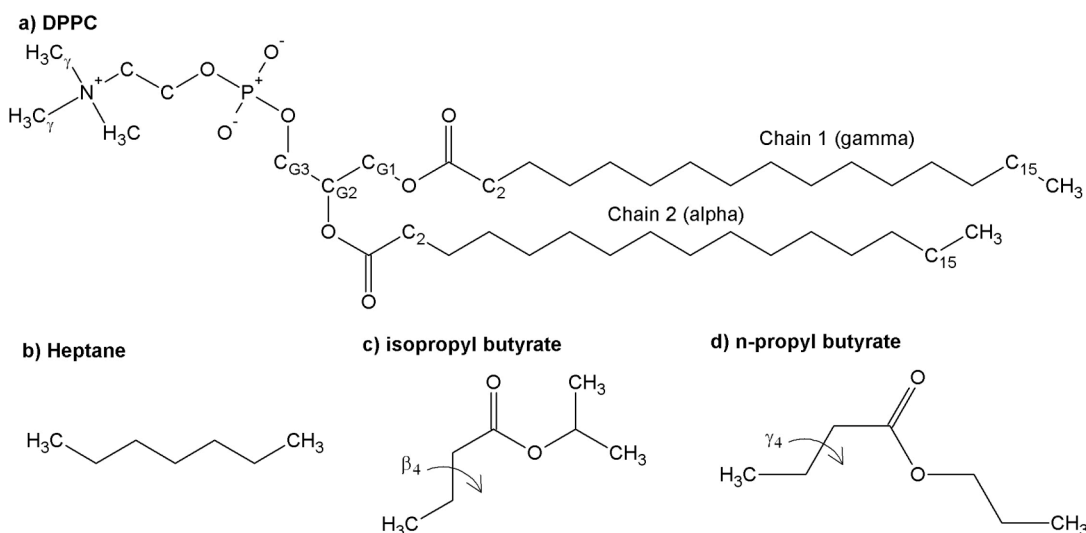


Figure 1. DPPC (a) and three of the compounds used to parameterize the lipid force field: (b) heptane; (c) isopropyl butyrate; (d) and *n*-propyl butyrate. Atom names for DPPC follows the *sn* IUPAC nomenclature (IUPAC, 1967). Torsions on the Chain 1 and 2 are labeled γ_i and β_i , respectively, following the Sundaralingam convention (Hauser et al., 1980; Sundaralingam, 1972). Specifically, β_4 and γ_4 are the C_1 - C_2 - C_3 - C_4 in the torsions in chain 2 and chain 1 of DPPC, respectively. The analogous torsion angles are noted in (c) and (d) for the model esters.

The inclusion of solvent effects on conformational energies is less straightforward than the basis set dependence on optimization. Atomistic MD simulations of hydrated lipid bilayers include the solvent effects directly with water models, such as TIP3P.

However, the accuracy of these models is limited to the two-body assumption, and this lack of polarizability may influence conformations of the solute. The solvation effect appears to be important in obtaining the correct anomeric energy ratios for carbohydrates (Woodcock et al., 2007). Therefore, more expensive QM energy calculations should be performed with solvent models, such as, polarizable continuum models (PCM) (Cances et al., 1997; Cossi et al., 2002) to test the validity of *in vacuo* calculations. For alkanes and esters, the solvation effects are minimal (Fig. 2). The small increase in the energy of g^- conformer with the β_4 torsion is within the uncertainty of the method. Similar results are found with solvated alkanes. These PCM calculations imply the validity of using *in vacuo* QM calculations of alkane and glycerol model compounds.

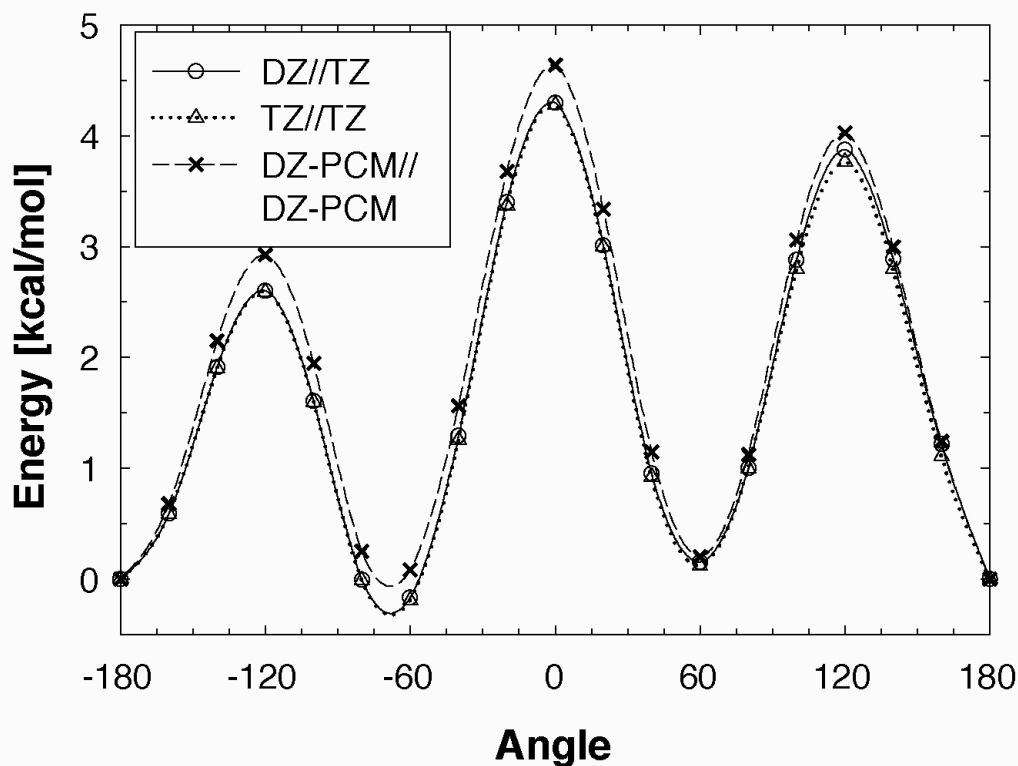


Figure 2. The $\text{CH}_3\text{-CH}_2\text{-CH}_2\text{-C=O}$ (β_4 in Fig. 1) surface of isopropyl butyrate from three methods: DZ = MP2/cc-pVDZ, TZ = MP2/cc-pVTZ, DZ-PCM = MP2/cc-pVDZ with solvent correction. The notation used is as follows: (optimized level) // (single point energy). This surface is a model for the β_4 torsion in DPPC.

The conformational energies as a function of dihedral angle are used to parameterize the CHARMM FF. The minimum energy structure of these conformers is determined using the Berny algorithm (Schlegel, 1982) to fix a desired dihedral angle and relax the remaining degrees of freedom. An example of a torsional surface scan is shown in Fig. 2 for isopropyl butyrate. Multiple torsional surface scans are used for alkanes so that conformations are sampled from t to g and tg to g^+g^+ to g^+g^- . This is especially important because adjacent gauche states are stabilized compared to staggered gauche states such as g^+tg^+ (Klauda et al., 2005b). After a minimum energy structure is determined for each conformation, Eq. (4) (MP2:CC) is used to obtain the energy effectively at CCSD(T)/cc-pVQZ, which is nearly the value at the basis set limit; the SBS used is cc-pVDZ and the LBS is cc-pVQZ.

The following objective function was used to obtain the alkane terms of C27r and the ester terms of the developmental force field, referred to here as C27r-a:

$$\chi = \sum_i^{\text{\# of QM points}} \left[U_i^{QM} - U_i^{Model} \right]^2 \quad (5)$$

where U_i and is the energy for conformation i . A minimalist approach is used when fitting the dihedral potential in Eq. (1) to the QM conformational energies in Fig. 3. The number of terms per dihedral (j) is limited to four, but initially fits with fewer terms are tested to minimize the number of parameters. Two to four terms are used for the C27r alkane force field, but fits to the ester conformation require four terms. The periodicity, n_j , in Eq. (1) is fixed as an integer and not allowed to be larger than six, which prevents overfitting to the QM energies. Similarly, the phase term δ_j is only allowed to be 0 or π . Fig. 3 includes the best fits to the QM configurations with the preceding parameter constraints. The C27r force field improves the alkane torsional profiles over C27, which was optimized targeting lower-level QM data, both by decreasing the transitional barriers and the increasing breadth of the *gauche* potential (Fig. 3, top). The other torsions in DPPC were left unmodified in the conversion from C27 to C27r, so it is expected that comparable shifts would be observed when *ab initio* calculations at the same level are carried out on these torsions. This is indeed the case for the ester torsions (Fig. 3, middle and bottom). For example, the transitional barriers for both β_4 and γ_4 are decreased by nearly 2 kcal/mol high, and the *gauche* minima are decreased about 0.7 kcal/mol.

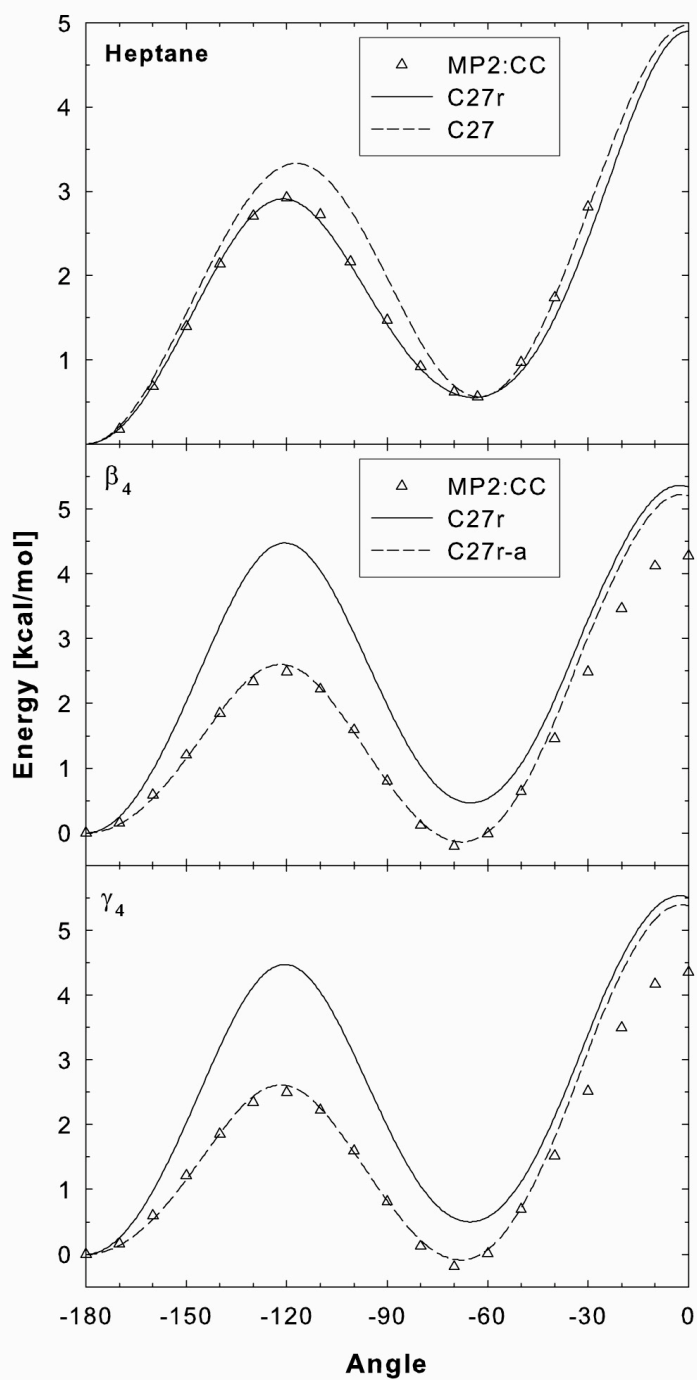


Figure 3. Conformational energies for the C2-C3-C4-C5 dihedral angle of heptane with all other dihedrals constrained to *trans* (top), and CH₃-CH₂-CH₂-C=O (the β_4 model) of isopropyl butyrate (middle) and *n*-propyl butyrate (the γ_4 model) (bottom). QM energies are at CCSD(T)/cc-pVQZ (defined MP2:CC in Eq. 4). The lines are the surfaces of the empirical potentials, including the developmental set C27r-a.

Consequently, populations of *gauche* conformers will be underpredicted with C27r. However, a simple adjustment to the torsional potential results in an excellent fit to the QM energies with only minor differences for the high energy *cis* state.

The methods described can be used to fit any torsional profile of interest. The alkane and ester torsions are simple and are parameterized independently; *i.e.*, the potential function for these torsions does not explicitly require the values of neighboring torsions even though different conformations of these neighbors may have been used for the fitting. This does not imply that the coupling between torsions is absent; it can be substantial and is manifested in the well-known “crankshaft” transitions of acyl chains in bilayers (Brown et al., 1995). More complex regions, such as a glycerol moiety, may require explicit coupling between neighboring torsions. This could be corrected by the CMAP modification currently used to parameterize the ϕ/ψ linkage in peptides.

C. Condensed phase simulations of model compounds

The next step in the development of the force field is extensive simulation of condensed phases of the model compounds and related molecules; these differ from the free energy simulations used to establish the nonbond parameters on small molecules (*e.g.*, ethane in water). Results for alkanes are presented here as illustration. Subsection C.3 compares bulk equilibrium properties (density and isothermal compressibility) for heptane, decane and tetradecane from C27, C27r and experiment; Subsection C.4 compares the nonequilibrium properties (diffusivity, viscosity, and ^{13}C NMR relaxation times). Subsection C.5 considers the alkane/air, water/air and alkane/water interfaces for C27r, and the TIP3P and TIP4P-Ew water models. Before proceeding to these results, some general comments on long-range interactions (II.C.1) and finite size effects (II.C.3) are necessary. The reader is referred to Klauda et al. (2005a) and Klauda et al. (2007) for further details on the material in this subsection.

C.1 Long-range forces

The current alkane CHARMM parameters were developed using Particle Mesh Ewald (Darden et al., 1993) (PME) to include long-range electrostatics, and the analytic long range correction (LRC) (Allen and Tildesley, 1987) for the long-range LJ terms. Hence, simulations using this FF should be carried out similarly. However, while PME is

applicable to multicomponent bulk and interfacial systems, the analytic long-range correction (LRC) corrections for LJ terms are only rigorously applicable to single component bulk systems. To circumvent this problem, most of the simulations to follow (including the DPPC bilayers) have been carried out using the pressure-based long-range correction (LRC) (Lagüe et al., 2004). Constant volume systems, such as alkane/vapor and lipid monolayers, cannot be directly simulated with the preceding LRC. For these the recently developed isotropic periodic sum (IPS) method (Wu and Brooks, 2005) was applied. 2-D IPS is recommended for small systems (*e.g.*, alkane/vapor and water/vapor), while the hybrid PME/IPS (PME for electrostatics and 3-D IPS for LJ) is more efficient for large systems such as monolayers. PME/IPS, though approximate because of isotropic averaging of long-range LJ forces near the interface, may also be applied to lipid bilayers. Though computationally inefficient, long-range LJ terms may be included accurately by using a very long cutoff (*e.g.*, 30 Å).

The TIP3P water model was developed with a short cutoff applied to electrostatic and Lennard Jones interactions. Therefore, in principle, it is inconsistent to simulate it with the modern methods described above. In practice, simulating with PME leads to fewer artifacts than simulating without it (Feller et al., 1996), and CHARMM parameters are now developed with PME. A reparameterization of TIP4P explicitly for simulations with Ewald summation, denoted TIP4P-Ew, has recently developed (Horn et al., 2004). Some results for TIP4P-Ew are included here to show the effects of water models on surface tensions, though TIP3P remains the recommended model for simulations with CHARMM parameters.

C.2 Finite size effects

It is critical to eliminate, or at least to account for, finite size effects when developing and testing parameters. These effects vary for different properties and systems and are often difficult to predict, so explicit testing is required. The system size dependence for heptane is small; *i.e.*, simulations with $N=64$, 128 and 512 molecules yield the same averages for almost all bulk properties. An important exception to the preceding size dependencies is the self-diffusivity (or translational diffusion constant), D_s , where even $N=512$ shows substantial finite size effects. Fortunately, a simple correction is available (Yeh and Hummer, 2004):

$$D_s = D_{PBC} + \frac{k_B T \xi}{6\pi\eta L} \quad (6)$$

where D_{PBC} is the diffusion constant evaluated from the simulation (in cubic periodic boundary conditions with box length L), η is the viscosity, and $\xi = 2.837297$. Eq. (6) is for bulk systems, and cannot be directly applied to lipid lateral diffusion in bilayers (Section III.C). Lastly, size dependence should be rechecked when evaluating surface properties.

C.3 Bulk phase equilibrium properties of alkanes

An obvious first test of a potential is to verify that the system does not freeze when simulated above its melting point. This is not a trivial condition. Simulations of tetradecane with the AMBER99 (Wang et al., 2000) force field led to a quasi-crystal. The configuration shown in Fig. 4 (left) formed between 0.5 and 1.5 ns, and remained stable for the total simulation time of 10 ns. In contrast, simulations with C27 and C27r correctly yield liquid densities without freezing (see Fig. 4, right).

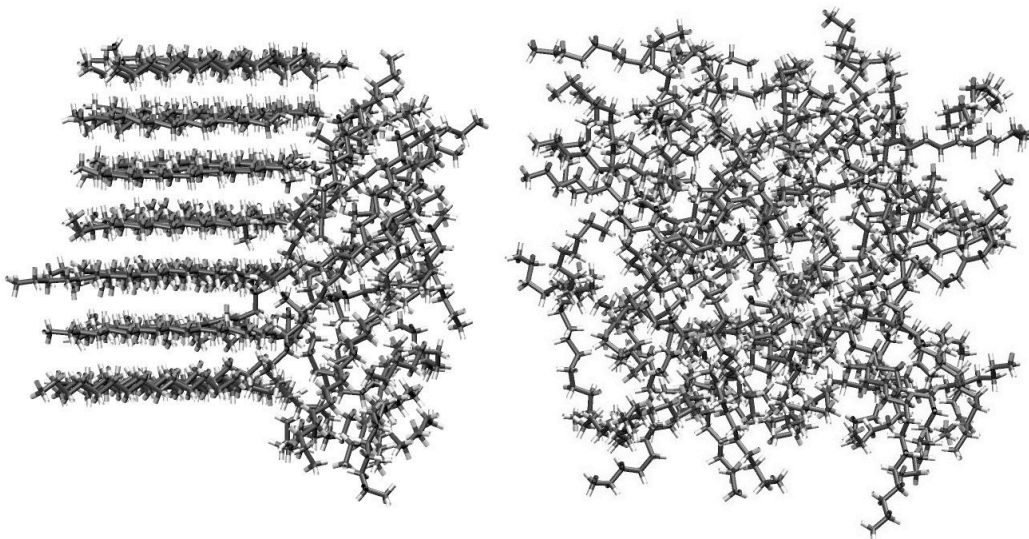


Figure 4. Snapshots of tetradecane simulated at 25 °C with the AMBER99 force field (left) and C27r (right) (Klauda et al., 2005a).

The density (ρ) and isothermal compressibility (β_T) directly probe the non-bonded contribution to the force field. Because these parameters are the same for C27 and C27r (only the torsional potential was adjusted), the results are expected to be very similar. The agreement with experiment for the density for alkanes is excellent: 1.0% for heptane

0.3% for decane, tridecane, and pentadecane (Table 1). However, neglecting the long-range LJ leads to 3% underestimate of the density.

Table 1. Simulation averages and standard errors for bulk properties of alkanes at 39 °C. Experimental values for density (ρ) and viscosity (η) from Small (1986); isothermal compressibility (β_T) from Lide (2000); and diffusivity (D_s) from Douglass and McCall (1958). D_{PBC} is the apparent self-diffusivity obtained directly from the mean-squared displacement in the simulations; the corrected self-diffusivity, D_s , is obtained from Eq (6).

		Alkane			
		C7	C10	C13	C15
ρ [g/cm ³]	C27r	0.661±0.014	0.712±0.012	0.740±0.010	0.755±0.009
	C27	0.660±0.015	0.712±0.011	0.741±0.010	0.755±0.009
	Exp.	0.668	0.716	0.743	0.755
β_T [10 ⁻¹⁰ m ² /N]	C27r	18.0±0.9	13.1±0.3	10.7±0.3	10.3±0.3
	C27	18.7±0.4	12.5±0.1	10.5±0.3	10.0±0.3
	Exp.	14.13	10.8	9.4	8.7
D_{PBC} [10 ⁻⁵ cm ² /s]	C27r	2.96±0.03	1.39±0.01	--	--
	C27	3.07±0.04	1.28±0.04	--	--
	Exp.	3.68	1.72	--	--
D_s [10 ⁻⁵ cm ² /s]	C27r	3.70±0.03	1.72±0.01	--	--
	C27	3.81±0.04	1.61±0.04	--	--
	Exp.	3.68	1.72	--	--
η [10 ⁻⁴ Pa s]	C27r	3.44±0.04	--	--	20.4±0.07
	C27	3.72±0.03	--	--	--
	Exp.	3.46	--	--	19.4

The isothermal compressibility (or its inverse, the bulk modulus K_b) is calculated from NPT simulations from the volume V and volume fluctuations $\langle \delta V^2 \rangle$,

$$\beta_T = K_b^{-1} = -\frac{1}{V} \left(\frac{\partial V}{\partial P} \right)_T = \frac{\langle \delta V^2 \rangle}{Vk_b T} \quad (7)$$

where k_b is Boltzmann's constant, and T is the temperature. The results are not as good as the densities: approximately a 30% overestimate of experiment for heptane, and 13-20% for the longer alkanes (Table 1). Neglecting the long-range LJ terms increases the errors substantially; *e.g.*, β_T is approximately 50% too high for heptane. The sensitivity of β_T to the LRC suggests the LJ terms as targets for further improvements in the force field.

C.4 Bulk phase nonequilibrium properties

Diffusion constants D_{PBC} were calculated as 1/6 of the long-time slope of the mean squared displacement versus time,

$$MSD(t) \equiv \frac{1}{N} \left\langle \sum_i (x_i(t) - x_i(0))^2 + (y_i(t) - y_i(0))^2 + (z_i(t) - z_i(0))^2 \right\rangle \quad (8)$$

where x_i , y_i and z_i are the positions of the center of mass of each particle. Self-diffusion constants D_s , with a finite size correction were then obtained from Eq. (6).

Table 1 shows both the substantial correction for system size, and the near perfect agreement experiment for D_s of heptane and decane.

The shear viscosity for heptane and pentadecane was calculated using the Green-Kubo formula (Allen and Tildesley, 1987),

$$\eta = \frac{V}{kT} \int_0^\infty \langle P_{\alpha\beta}(t) P_{\alpha\beta}(0) \rangle dt \quad (9)$$

where $P_{\alpha\beta}$ are the off-diagonal elements of the instantaneous pressure tensor. Since pressure is a system property, a high sampling rate and a simulation time of at least 10 ns is required to obtain accurate shear viscosities. As might be expected from the good agreement demonstrated for the diffusion constants, the calculated viscosity from C27r for heptane matches experiment, and pentadecane overestimates experiment by only 5% (Table 1). As follows from the potential surfaces (Fig. 3 top), C27r yields somewhat more flexible chains than does C27. This plausibly explains the higher viscosity of heptane for C27.

The most dramatic difference between C27 and C27r is the NMR ^{13}C T_1 relaxation times. This is because NMR ^{13}C T_1 relaxation in liquid alkanes arises from a combination of molecular tumbling (which sensitive to the viscosity and molecular shape) and isomerization (which is sensitive to the torsional barriers) (Zhang et al., 1996). Assuming that relaxation is due to dipolar interactions between the ^{13}C nucleus and its N attached protons, the ^{13}C T_1 is

$$\frac{1}{NT_1} = \frac{1}{10} \left(\frac{\hbar\gamma_c\gamma_h}{r_{C-H}^3} \right)^2 [J(\omega_H - \omega_C) + 3J(\omega_C) + 6J(\omega_H + \omega_C)] \quad (10)$$

where \hbar is Plank's constant divided by 2π , r_{C-H} is the effective C-H bond length, γ_H, γ_C , ω_H , and ω_C are the gyromagnetic ratios and Larmor frequencies, respectively, of the ^{13}C and ^1H nuclei; $\omega_C = \gamma_C H$ and $\omega_H = \gamma_H H$, where H is the field strength. $J(\omega)$ is the spectral density of the second rank reorientational correlation function:

$$J(\omega) = \int_0^\infty \langle P_2(\hat{\mu}(0) \cdot \hat{\mu}(t)) \rangle \cos(\omega t) dt \quad (11)$$

where P_2 is the second order Legendre polynomial and $\hat{\mu}(t)$ is the unit vector along the CH bond direction at time t . The T_1 's of liquid alkanes are independent of the magnetic field strength (Brown et al., 1983; Lyerla et al., 1974). This occurs when all of the components of $\langle P_2(\hat{\mu}(0) \cdot \hat{\mu}(t)) \rangle$ decay rapidly compared to $1/\omega_H$, and the molecule is said to be in the motional narrowing regime. Assuming motional narrowing, and setting $r_{C-H} = 1.117 \text{ \AA}$ (Ottiger and Bax, 1998), Eq. (10) reduces to

$$\frac{1}{NT_1} = (1.855 \times 10^{10} \text{ s}^{-2}) \int_0^\infty \langle P_2(\hat{\mu}(0) \cdot \hat{\mu}(t)) \rangle dt = (1.855 \times 10^{10} \text{ s}^{-2}) \tau \quad (12)$$

where τ is the rotational correlation time.

Figure 5 compares the calculated and experimental relaxation times for pentadecane. T_1 's for C27r agree very well except for the end of the chain, while those from C27 are uniformly low. This is consistent with the relative *trans-to-gauche* barrier heights for the two FF (Fig. 3, top). The lower barrier for C27r leads to more isomerizations, lower relaxation times, and, from Eq. (12), higher T_1 's than C27. Results for shorter alkanes do not agree as well with experiment. This likely results from overly fast rotation about the long molecular axis. However, discrepancies for short alkanes are not a large concern for development of a lipid FF, because the acyl chains in a lipid are tethered to the head group and thereby cannot rotate about their long axes.

The changes to the dihedral potential also modulate the population of *trans* and *gauche* states in alkanes. There is limited experimental data available to compare the dihedral populations but, on average, C27r results in a 5% increase over C27 in the *gauche* population for all alkanes. Experimentally, Fourier transform infrared (FT-IR)

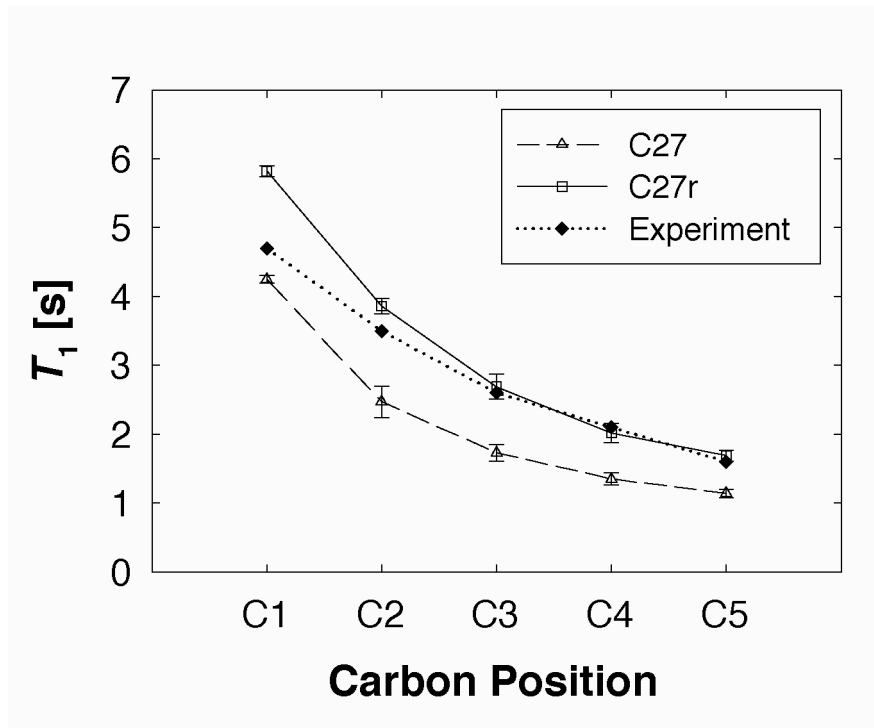


Figure 5. T_1 relaxation times of pentadecane from simulation (Klauda et al., 2005a) and experiment (Lyerla et al., 1974).

spectroscopy can be used to determine the fraction of conformational states in alkanes. For tridecane, Holler and Callis (1989) measured 3.5 *gauche* bonds per molecule and simulations with C27 and C27r result in 2.75 and 3.04, respectively. The fraction of *trans* states with C27r for alkanes larger than decane are nearly independent of chain length with a value of 0.70, in agreement with results of Karaborni and O'Connell (1990) who obtained a fraction *trans* of 0.69 essentially independent of the chain length.

C.5 Interfacial properties

The surface tension, γ , provides insight into the anisotropic forces at interfaces, and its calculation is a standard part of testing CHARMM parameters. For a planar interface whose normal is parallel to the z -axis, γ , is defined as follows:

$$\gamma = \int_{-\infty}^{+\infty} (P_N - P_T(z)) dz \quad (13)$$

where P_N and P_T are the normal and tangential components of the pressure tensor. Because $P_N = P_T$ in the bulk, the integrand is only positive in the region of the interface. For a planar interface, P_N is independent of z and equals the bulk pressure P , so it

follows from Eq. (13) that the tangential pressure is negative in the interfacial region. In fact, it is quite negative. The surface tension of the hexadecane/water interface is approximately 50 dyn/cm. Assuming the interfacial thickness is 10 Å, the average tangential pressure in the interface is therefore -500 atm.

Surface tensions in CHARMM are evaluated from the components of the stress tensor across the simulation cell (Zhang et al., 1995),

$$\gamma = 0.5 \langle L_z [P_{zz} - 0.5(P_{xx} + P_{yy})] \rangle \quad (14)$$

where L_z is the instantaneous height. The factor of 0.5 is included to take into account that the fluid is simulated as a slab and, by construction, there are two interfaces in the simulation cell. This definition works well for simple interfaces and monolayers, but is awkward for bilayers. To avoid ambiguity, the units for bilayer surface tension for bilayers are reported as dyn/cm/side.

Surface tensions of liquid/vapor interfaces, including lipid monolayers, are evaluated in the NVT ensemble (constant particle number, volume and temperature). No fluctuations in the cell dimensions are necessary. Liquid/liquid interfaces are most easily simulated in the $NPAT$ ensemble, where P in this context indicates the normal pressure, and A is surface area. This allows the cell height to adjust, and the densities in the centers of the fluid slabs to relax to their bulk values.

Surface tensions converge relatively rapidly in simulations of most liquids. A precision of one dyn/cm can be obtained for simple interfaces (alkane/water and alkane/air) in several ns. As for the isothermal compressibilities, long-range LJ interactions are important and must be included for quantitative assessments of the potential. From Table 2, approximately half of the surface tension of alkane/vapor interfaces is attributable to long-range LJ terms. Once treated correctly, the surface tensions of alkanes are in excellent agreement with experiment. Both TIP3P and TIP4P-Ew underestimate the surface tension of water by 23% and 15%, respectively. The errors in surface tension of hexadecane/water are -10% for TIP3P and +8% for TIP4P-Ew. Hence, interactions of water and alkane that take place on the boundary of the acyl chains of the bilayer and waters solvating the head groups are reasonably, but not quantitatively, described, in the CHARMM lipid FF.

Table 2. Surface tensions (in dyn/cm) calculated with a 10-Å cutoff for Lennard-Jones interactions, with long range LJ interactions included by the IPS method, and experiment (Small, 1986) for alkane and alkane/water (Joart and Martinek, 2007; Lemmon et al., 2005) for water). Long range electrostatics were included with PME for all simulations.

System	Without long-range LJ	With long-range LJ	Expt
heptane (25 °C)	9.0	18.7	19.8
hexadecane (50 °C)	12.1	25.2	25.0
water (TIP3P, 50 °C)	45.7	52.2	67.9
water (TIP4P-Ew, 50 °C)	53.2	57.4	67.9
hexadecane/water (TIP3P, 25 °C)	44.9	48.2	53.3
hexadecane/water (TIP4P-Ew, 25 °C)	53.4	57.3	53.3

III. Membrane Targets and Related Issues

Most of the results described in this section are for DPPC at 50°C. While unsaturated lipids are more common in biological membranes and are available in CHARMM, the wealth of experimental data available for DPPC make it a prime target for parameter testing and development. The systems generally contain 72-80 fully hydrated lipids, and were simulated for 50-100 ns at a surface area fixed to the experimental value of 64 Å²/lipid. Important exceptions are noted, and the details can be found the original references.

A. X-ray diffraction of liquid crystals and structural models

X-ray and neutron diffraction provide critical structural observables: the bilayer thickness and area, and the density distributions of its components. While comparisons with Fourier reconstructions (Levine and Wilkins, 1971), D-spacing (Lewis and Engelman, 1983; Rand and Parsegian, 1989), average atom positions (Buldt et al., 1979; Zaccai et al., 1979) have proven useful, the most rigorous comparison of simulation and experiment is through the structure factors, $F(q)$ (Benz et al., 2005; Nagle and Tristram-Nagle, 2000). These are related to the total lipid density $\rho(z)$ by

$$F(q) = \int_{-D/2}^{D/2} [\rho(z) - \rho_w] \cos(qz) dz \quad (15)$$

where ρ_w is the electron density of pure water, and D is the length of the unit cell perpendicular to the bilayer normal. Figure 6 compares the results of C27 and C27r with

experiment. Both parameter sets yield the experimental positions of the first three lobes ($q=0.16, 0.35$ and 0.52). The root mean squared deviation (RMSD) with experiment can provide a convenient metric for ranking. In this case, however, partly because of the relatively large experimental errors at high q and the similarity of C27 and C27r, the RMSD of the two FF are comparable.

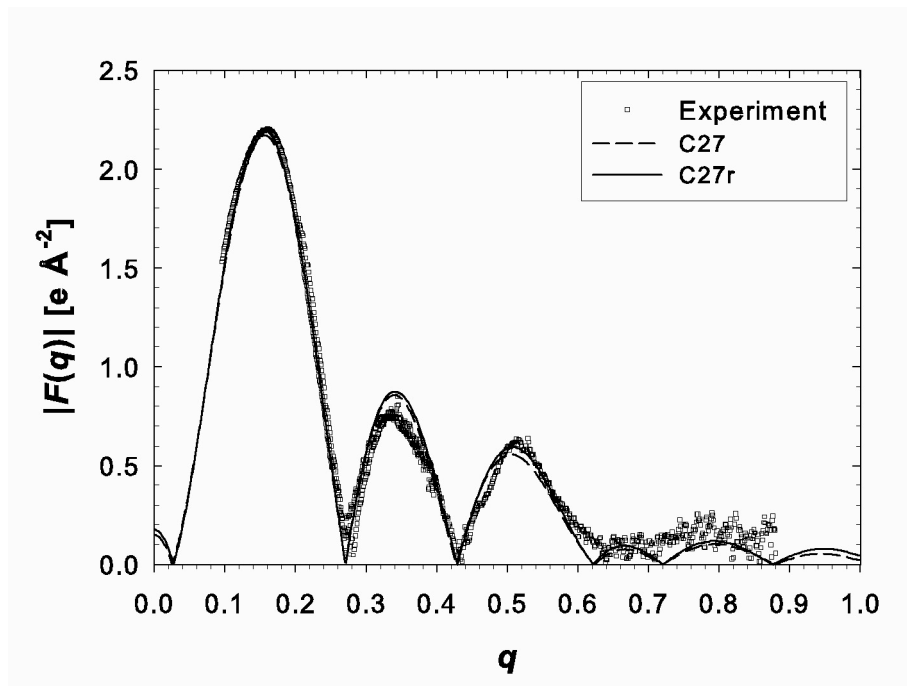


Figure 6. Form factors $F(q)$ for DPPC from simulation (Klauda et al., 2007) and experiment (Kučerka et al., 2006).

Structure factors are very sensitive to the surface area per lipid, and can be used to estimate surface areas from simulation. For example, simulations of dimyristoylphosphatidylcholine (DMPC) bilayers were carried out at a range of surface areas that bracket the value of $60.6 \text{ \AA}^2/\text{lipid}$ obtained (with some assumptions) from the experimental data. The RMSD in $F(q)$ from simulation and experiment equaled 0.22 ± 0.007 , 0.072 ± 0.007 , 0.044 ± 0.003 , 0.047 ± 0.002 , 0.12 ± 0.001 , at 55.0 , 59.7 , 60.7 , 61.7 and $65.0 \text{ \AA}^2/\text{lipid}$, respectively. Hence, differences of $1.0 \text{ \AA}^2/\text{lipid}$ can be distinguished in cases where the quality of the experimental data is high. Furthermore, the best agreement was obtained by the simulation with a surface area ($60.7 \text{ \AA}^2/\text{lipid}$) nearest to experiment. The success of this exercise provides further support for the CHARMM FF. It also implies that simulations (with a well validated FF) can be

combined with experimental diffraction data to obtain surface areas for multicomponent bilayers Klauda et al. (2006b). This is a welcome advance because these areas are very difficult to obtain from experiment alone.

An important thrust in present day analysis is the comparison of the densities of the individual membrane components from experiment and simulations. While the component densities are easy to calculate from simulation, extracting them for experiment is not straightforward, especially for fully hydrated systems. This is because the component densities are not directly observed. Rather, they must be related to the total density by a “structural model”, such as the following (Klauda et al., 2006b):

$$\rho(z) = \rho_P(z) + \rho_{CH_3}(z) + \rho_{CG}(z) + \rho_{CH_2}(z) + \rho_{BC}(z) \quad (16)$$

where $\rho_P(z)$ is for the phosphate groups, $\rho_{CH_3}(z)$ for the terminal methyls, $\rho_{CG}(z)$ for the carbonyl+glycerol, $\rho_{CH_2}(z)$ for the methylenes on the hydrocarbon chains, and $\rho_{BC}(z)$ for the water+choline (BC). The functional forms are assorted Gaussian and error functions, and require a total of 11 parameters. This is reduced to 5 by introducing data (*e.g.*, the lipid molar volume) and selected assumptions. Practically the large number of parameters/constraints makes it difficult to deduce component densities without some ambiguity.

In spite of these limitations, a component analysis provides a very useful test of the simulation. Figure 7 shows the results for DPPC. It is clear that the major features of the density, the phosphate peak and the methyl trough, are largely reproduced, though a careful analysis of the latter reveals that experiment and simulation are statistically different. Is the present 7% disagreement of simulation and experiment for the total density in the bilayer midplane acceptable, or is there reason to try to do better? The component analysis indicates that the agreement is partly the result of cancellation of errors: the methyl density is 21% low and the methylene is 25% high. Such difference is of greater concern, and will be monitored in future parameter development. Other discrepancies include the water distribution, which partially reflects the approximations inherent in the TIP3P water model.

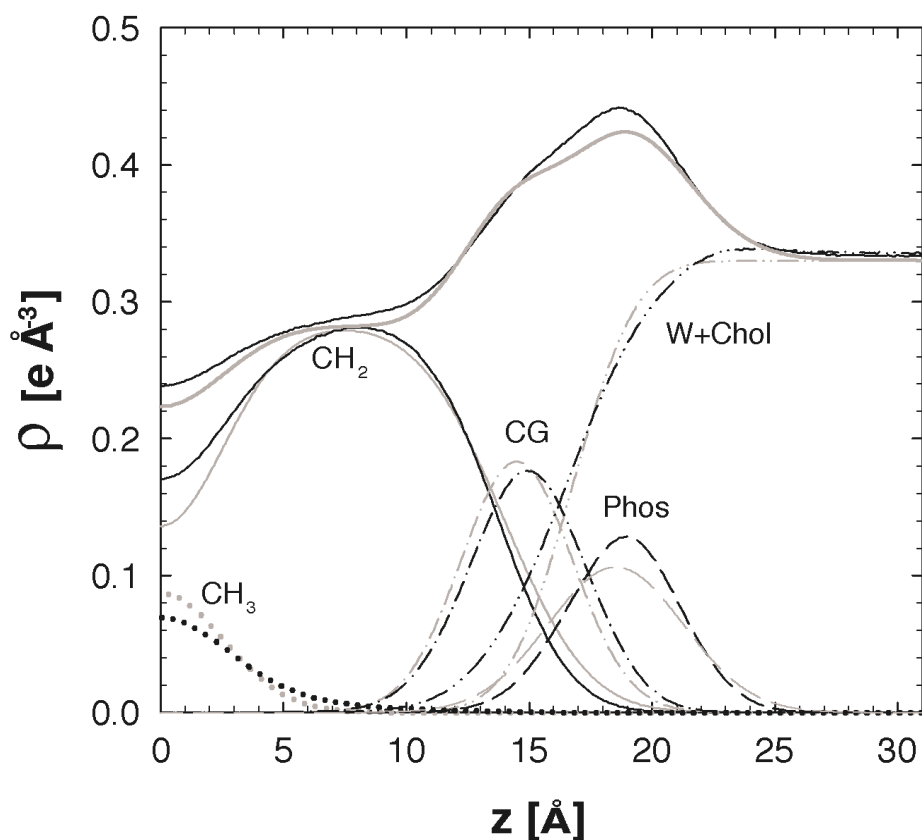


Figure 7. The electron density of the DPPC bilayer from simulation (black) (Klauda et al., 2007) and experiment (Kučerka et al., 2006) (grey). The individual component densities are also shown: CH₃=methyl, CH₂=methylene, CG=carbonyl-glycerol, P=phosphate, and W+Chol=water and choline.

While C27r yields nearly quantitative agreement with experiment for fluid phase DPPC and DMPC at the experimental surface area per lipid, the situation with gels is less clear. The gel phase is tightly packed and motion is restricted, making equilibration difficult. The utility of the gel phase as a target for parameterization is limited until these issues are resolved.

B. Deuterium order parameters and the signature at C2

The deuterium order parameter, S_{CD} , provides an indispensable measure of both disorder and fine-structure in lipid bilayers. However, its interpretation is not entirely straightforward, and values calculated in simulation do not necessarily correspond to

quantities that can be measured. The subsection attempts to clarify some potential misconceptions and highlights a target that deserves more attention.

Experimentally, a fraction of the hydrogens at selected carbons are replaced by deuteriums, and the residual quadrupolar coupling of the CD bond is measured. If the CD bond is axially averaged about a director, the spectrum will appear as a symmetric powder pattern (Seelig, 1977). S_{CD} is proportional to the distance between peaks (or splitting, $\Delta\nu$) in the powder pattern and is related to angle θ that the CD bond makes with the director by

$$S_{CD} = \left\langle \left| \frac{3\cos^2\theta - 1}{2} \right| \right\rangle \quad (17)$$

where the brackets signify an average over all orientations. The coincidence of the director and normal has been established for fluid phase bilayers using measurements on oriented samples, so θ can be assumed to be the instantaneous angle of the CH vector and the bilayer normal in most applications. The absolute value signs, which are not always included in definitions, are included here as a reminder that S_{CD} , like $\Delta\nu$, is always positive. Residual dipolar couplings of CH and HH can be negative (Gross et al., 1997), and therefore contain additional information.

To a reasonable approximation, S_{CD} can be written as the product of three order parameters:

$$S_{CD} = S_{\text{int}} \times S_{\text{wobble}} \times S_{\text{collective}} \quad (18)$$

where S_{int} is associated with internal motions such as *gauche-trans* isomerization, S_{wobble} arises from the rigid-body diffusive rotation motion of single lipids sometimes denoted as “wobble in a cone”, and $S_{\text{collective}}$ comes from collective rotations of groups of lipids. However, S_{CD} only reflects motions that are averaged on the time scale of deuterium quadrupolar coupling constant, 170 KHz, or approximately 10^{-5} s. Hence, very slow collective motions (*e.g.*, those on the second time scale) do not contribute the average in Eq. (17).

The preceding conditions place some restrictions on simulators. For example, DPPC gels are known *not* to be axially averaged (Davis, 1983), so reporting S_{CD} from a

simulation of a gel is inappropriate. In principle, axial averaging (or its absence) can be demonstrated. If the z -axis is taken to be the axis of averaging, axial averaging implies that the averages $\langle \hat{x}^2 \rangle = \langle \hat{y}^2 \rangle$, and $\langle \hat{x} \rangle = \langle \hat{x}\hat{y} \rangle = \langle \hat{x}\hat{z} \rangle = \langle \hat{y} \rangle = \langle \hat{y}\hat{z} \rangle = 0$, where the “hat” signifies the appropriate unit vector projections. In effect, the lipid rotationally diffuses about the z -axis and averages out the x and y projections within 10^{-5} s. Clearly it is not practical to demonstrate that a gel is not axially averaged at present, though it is easy to demonstrate axial averaging for the fluid state.

Present simulations of lipid bilayers are usually on the 50-100 Å length scale, and 10-100 ns time scale. Consequently, motions on larger length scales (*e.g.*, 1000 Å) whose time scales *are* well averaged on the 10^{-5} s time scale would not be observed in simulations of a small system because of constraints imposed by periodic boundary conditions. If the contribution of such motions to S_{CD} is not negligible, the agreement with experiment obtained for small systems is fortuitous.

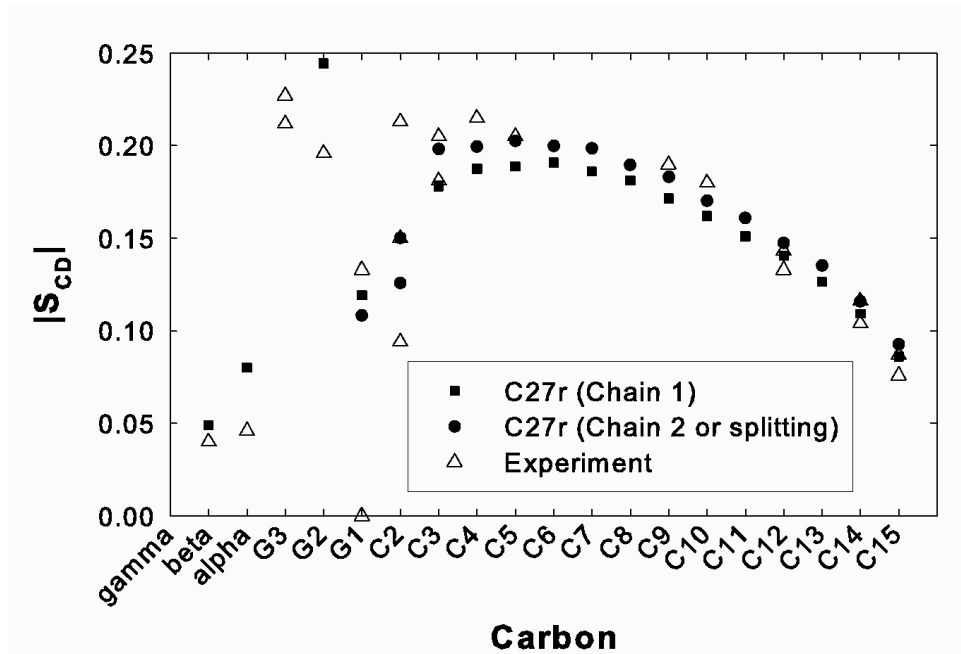


Figure 8. Deuterium order parameters for DPPC from simulation ((Klauda et al., 2005a) for chains; glycerol and headgroup unpublished) and experiment ((Gally et al., 1981; Seelig and Seelig, 1974; Seelig and Seelig, 1975; Seelig et al., 1977))

The experimental and simulated order parameters for DPPC are plotted in Fig. 8. There are two very characteristic features of the order parameter profile. The first is a

plateau region for the chain carbons extending from carbonyl region to around carbon 10, followed by a drop-off to lower values. The value of the plateau region, approximately 0.2, indicates intermediate disorder, and is a basic target for any force field. While the decomposition of S_{CD} into its components is approximate, a range of 0.6-0.7 for S_{wobble} appears reasonable (Feller et al., 1997a). Assuming that the contribution of collective motions is small, $S_{int} = 0.29-0.33$ for the plateau, and it drops further down the chain. S_{int} for these carbons is largely determined by the quality of the alkane potential, which highlights the utility of parameterizing the FF from the molecular fragments. Like $F(q)$, S_{CD} is sensitive to the surface area per lipid (Feller et al., 1997a). This dependence appears more related to S_{wobble} than S_{int} for small deviations about the experimental area, and has a simple interpretation. A medium length alkane such as hexadecane rapidly isomerizes and tumbles in all directions; *i.e.*, there is no residual anisotropy. In a bilayer, the acyl chains isomerize and have similar conformational distributions as alkanes (Fig. 9). The difference in the two environments (from the perspective of the hydrocarbons) is that the chains of lipids are tethered at one end to the bilayer/water interface, while those in the alkane/water are not constrained in this manner. Expansions in the bilayer area are compensated by contractions in the bilayer thickness, leaving the bilayer interior substantially unchanged. However, wobbling is restricted. An expansion in the area increases the effective wobble angle, and thus decreases S_{wobble} .

The other characteristic feature is the splitting at carbon 2 on chain 2 (values of 0.09 and 0.15). Carbon 2 of chain 1 ($S_{CD}=0.205$), in contrast, groups with the other carbons in the plateau region. This inequivalence of the chains has been observed in numerous deuterium studies of both saturated and unsaturated lipids (Davis, 1983; Seelig, 1977), and appears to be critical structural feature of bilayers in their liquid-crystal phase. Given the striking “chair-like” structure in the glycerol region of lipids in their crystal forms (Pascher et al., 1992), some residual inequivalence of the chains might be expected. Therefore, it is disconcerting that C27r (and most current force fields) does *not* reproduce this feature of the order parameter profile. Rather, $S_{CD} \approx 0.16$ for all 4 CH vectors at carbon 2. A substantial spitting at C1 of the glycerol (labeled G1 in Fig. 8) is also not reproduced by the parameter set.

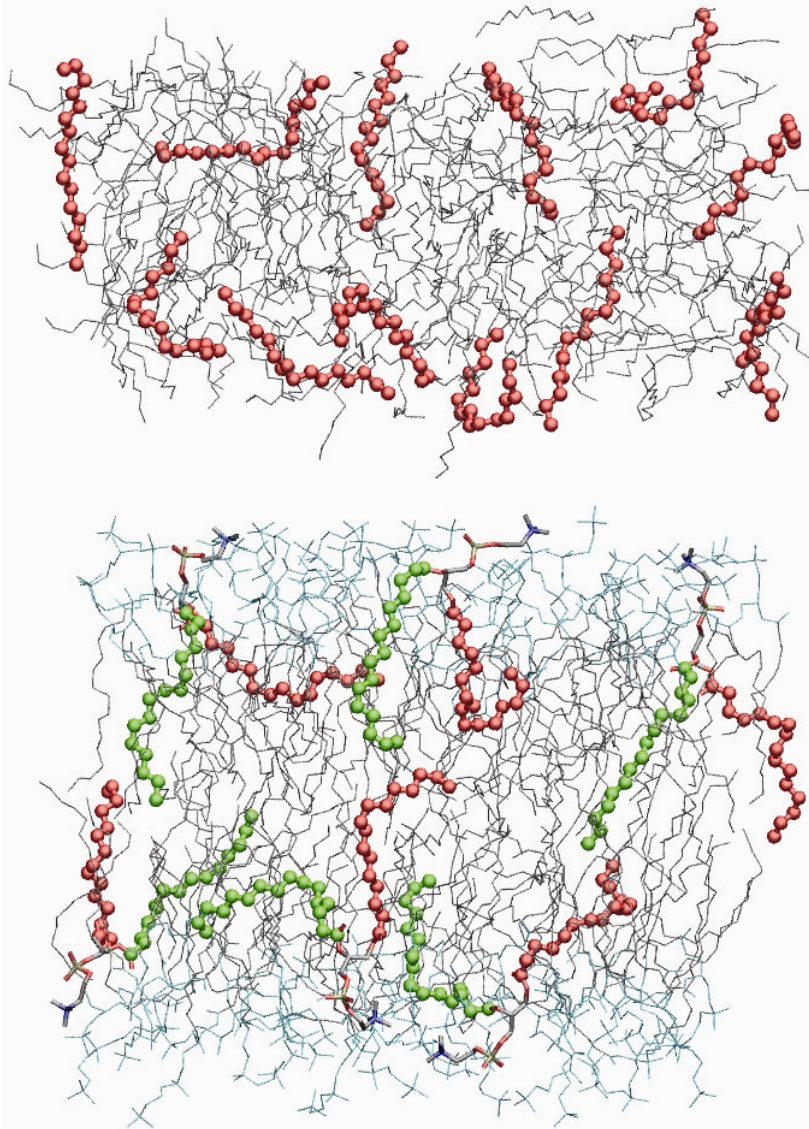


Figure 9. Snapshots from simulations of hexadecane/water (top) and a DPPC bilayer (bottom). 12 chains are highlighted in each graphic (chains 1 and 2 of DPPC are colored green and red, respectively), and the waters are omitted for clarity.

The order parameters of the other glycerol carbons and the head group are reasonably obtained. It is possible that very specific interactions, such as hydrogen bonds between the chain 1 carbonyl and the hydrogen on C2 of chain 2, promote the observed pattern. Such interactions are difficult to treat accurately in additive force fields.

C. NMR spin-lattice relaxation times and possible collective effects

Just as the deuterium order parameter probes the conformational preference of specific carbons of lipids in membranes, the spin lattice (or T_1) relaxation time yields information on the underlying dynamics. Values even at a single frequency are useful. Measurements taken at multiple fields enable a decomposition of the dynamics into fast and slow motions, and offers further targets for parameterization. Conversely, motional models are typically required to relate experimental decay constants to specific motions. Simulations are very useful in this regard, as the applicability of a motional model can be evaluated and alternative models examined. ^{13}C T_1 are the focus here, though other NMR relaxation data such as deuterium (Brown et al., 2002) and ^{31}P T_1 's (Roberts and Redfield, 2004) are also being used for testing.

As already noted in Section II.3, T_1 's of liquid alkanes are independent of the magnetic field strength. In contrast, $\langle P_2(\hat{\mu}(0) \cdot \hat{\mu}(t)) \rangle$ for lipids in bilayers contains multiple decays, including fast “alkane-like” ones. Hence, an important step in the validation of a lipid FF is a demonstration that experimental T_1 's for liquid alkanes comparable in length to the acyl chains of lipids are reproduced. This was described in Section II.C.4 for C27r.

Figure 10 shows the overall very good agreement of simulated (calculated from Eq. 10) and experimental T_1 's for DPPC at 500 MHz, including the alkane-like region near the bilayer midplane, and the more restricted head group/water interface. For carbons where both vesicle and multilayer data are available, simulations with C27r tend to be closer to the latter. This is encouraging, in that the multilayers are flat on a large length scale and thereby correspond more closely with the simulation geometry (where periodicity enforces flatness). The discrepancy of simulation and experiment at C3 is interesting. The simulated T_1 is too low, implying that motion is too slow. From Fig. 1, the dynamics of C3 is directly impacted by the β_4 and γ_4 torsional surfaces, which, from Fig. 3 (middle and bottom), contains a *trans-to-gauche* barrier that is approximately 2 kcal/mol too high for C27r. It is reasonable to anticipate that these changes will lead to faster dynamics and thereby better agreement with experimental T_1 's at C3.

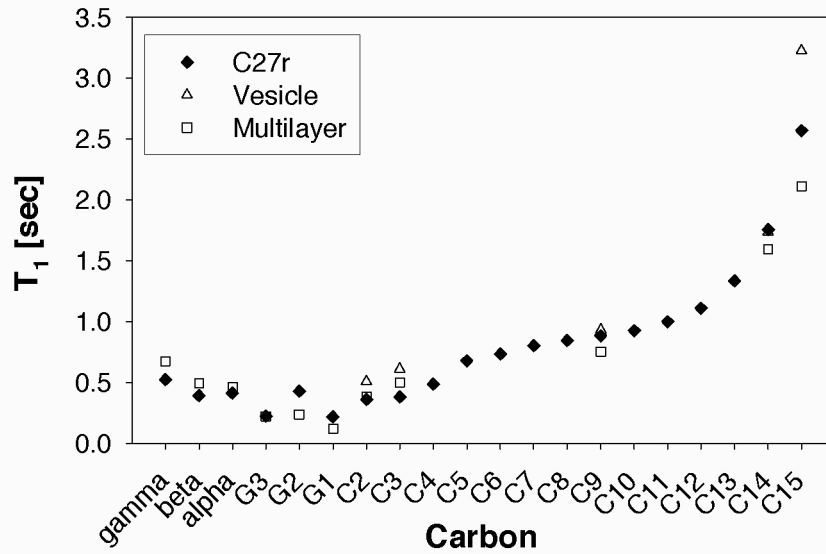


Figure 10 Spin lattice relaxation times at 500 MHz (hydrogen) for C27r and experiments on vesicles (Brown et al., 1983) and multilayers (Gawrisch and Eldho, unpublished data). The experimental points at C9 are the average of C4-C13. T_1 's for the acyl chain carbons are averaged.

The vesicle data of Brown et al. (1983) was obtained at a very wide range of frequencies. While its interpretation has been somewhat controversial, it has proven very valuable to the development of the field. As shown Fig. 11, the data for the average of carbons 4-13 (taken from 15 to 125 MHz) are remarkably linear when plotted versus $\omega_c^{-1/2}$; $1/T_1$ for the other carbons show similar behavior. This dependence was interpreted by Brown to indicate collective motions. Szabo (1986) analyzed the same data with a “model-free” formalism (Lipari and Szabo, 1982), where the spectral densities (Eq. 10) are written:

$$J(\omega) = (1 - A_j^2)\tau_j + \frac{A_j^2\tau_s}{1 + (\tau\omega)^2} \quad (19)$$

where τ_j is a fast relaxation time for each carbon and A_j^2 is the generalized order parameter (not to be confused with deuterium order parameter), and τ_s is a slow relaxation common to all of the carbons. A single slow relaxation time is more consistent with single lipid diffusive reorientation than with collective motion. (Restricted diffusion leads to multiexponential decays (Szabo, 1984), but one tends to dominate.) The

excellent fit of Eq. (19) to the experimental data (Fig. 1, dotted line) indicates that a non-collective model for the frequency dependent T_1 's is at least plausible in this frequency range. The results of Brownian and MD simulations (Pastor et al., 2002) support this proposal, and have associated τ_s with a pendulum-like diffusive orientation (or “wobble”) of individual lipids.

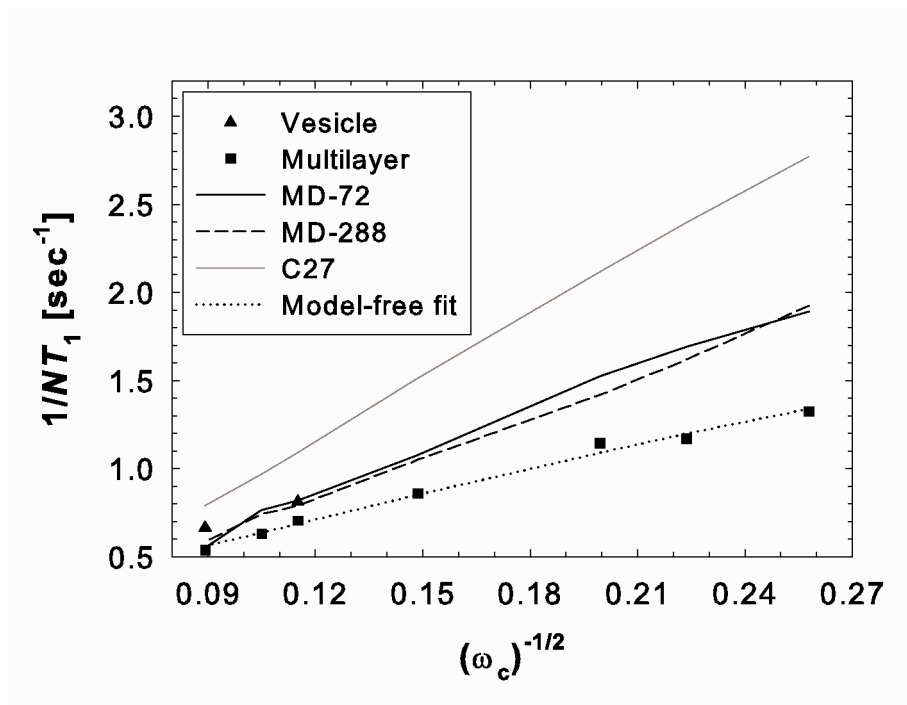


Figure 11 $1/T_1$ vs. $\omega_c^{-1/2}$ of carbons 4-13 (averaged) for experiments on vesicles (Brown et al., 1983), multilayers (Gawrisch and Eldho, unpublished data), simulations with C27r at two system sizes, and C27 (Pastor et al., 2002), and a model free fit to experiment (Eq. 19) with $A_j^2 = 0.035$, $\tau_j = 24.5$ ps and $\tau_s = 2.1$ ns. The model-free parameters published earlier (Szabo, 1986), $A_j^2 = 0.035$, $\tau_j = 20.4$ ps and $\tau_s = 1.8$ ns, were obtained with $r_{C-H} = 1.1$ Å and thereby differ somewhat from those obtained here ($r_{C-H} = 1.117$ Å).

The fast relaxation times obtained by Szabo’s analysis have been quantitatively reproduced in MD simulations (Pastor et al., 2002), which has further validated the alkane parameters and confirmed the proposal of Brown that the fast dynamics corresponds to torsional dynamics of the acyl chains. However, as evident in Fig. 11, C27 does not lead to the observed frequency dependence. This discrepancy can be explained in three ways: (1) C27 is inadequate; (2) the simulation system (72 lipids) is

too small; (3) the data contain artifacts because of the high curvature the vesicles, which are only about 250 Å in diameter. Recent results suggest that the answer is a combination of (1) and (3). Specifically, T_1 's from the multilayers are uniformly lower than for the vesicles (Fig. 10). Simulations with C27r with 72 and 288 lipids yield almost identical T_1 's (Fig. 11), and they are in substantially better agreement with both multilayer and the vesicle data. While this does not rule out collective motions on longer length/lower frequency scales, it points to errors in the C27 FF. The argument is analogous to that provided for pentadecane in Section II.C.4: the *trans-to-gauche* barrier of C27 is 0.5 kcal/mol too high, which would decrease the fast component of T_1 , and lead to the overestimate of $1/T_1$ shown in Fig. 10. The barrier is reduced for C27r, and the agreement with experiment at high field is substantially improved. The frequency dependence for C27r is also in closer agreement with experiment than for C27. This can partially be explained by the broadening of the torsional potential influenced by the revision of C27. This broadening and the increased isomerization rate amplify the contribution of fast motions to the spectral density (A_j^2 is reduced in Eq. 19), and the apparent slope in a plot of $1/T_1$ vs. $\omega_C^{-1/2}$ is decreased. A final resolution of the discrepancy of simulations must await further improvements in the FF, simulations of larger systems including vesicles, and NMR measurements of DPPC multilayers at lower fields. Nevertheless, the calculation of ^{13}C T_1 's provides an important assessment of a parameter set.

D. Translational diffusion constants and a finite size effect

Experimental values of the lateral translational diffusion constant, D_ℓ , for lipids in bilayers have been available for many years, but it is only until recently that simulations could be carried out for sufficient lengths to calculate them. The slope of D_ℓ is obtained from the mean squared displacement in the xy plane vs. time, which equals $4 \times D_\ell$, analogous to translational diffusion in a bulk phase (Eq. 8). Adjustment for net translation of each monolayer is neither necessary nor recommended. Figure 12 plots the MSD from simulations of 72 and 288 lipids. Three features are evident: (1) The short-

time slopes of the two systems are similar; (2) they differ from the long-time slopes; (3) the long-time slopes are very different from each other.

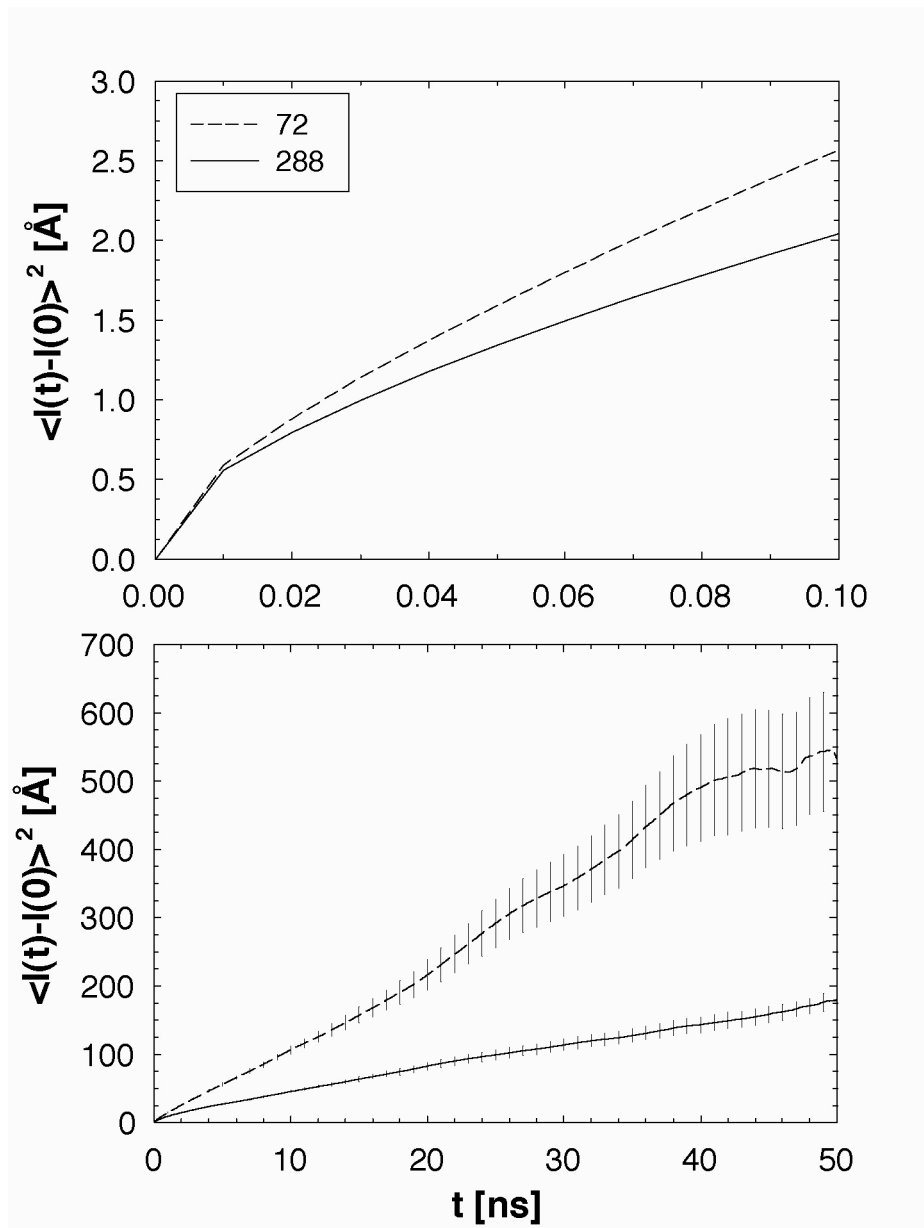


Figure 12. The lateral mean squared displacement of the center of mass of lipids for systems of 72 and 288 lipids over the intervals 0-100ps (top) and 0-50ns (bottom). Standard errors are denoted with vertical bars (Klauda et al., 2006a).

The first two features are easy to understand from Fig. 13, which plots the CM trajectory of one of the lipids from the system containing 288 lipids. The CM fluctuates in a local region and then makes two jumps to other regions in the 50-ns trajectory.

Others lipids make different numbers of jumps, as expected from a Poisson process, but the qualitative behavior is similar. This is the underlying reason for the two slopes in MSD: the local motion yields the rapid increase at short time; the infrequent (though substantial) jumps produce the smaller slope at long times. Strictly speaking, there is only a single translational diffusion constant for the system, and this is related to the long-time slope. It can be measured by NMR or photobleaching. The experimental values of $1.25 \times 10^{-7} \text{ cm}^2/\text{s}$ at $50 \text{ }^\circ\text{C}$ (Vaz et al., 1985) and $1.52 \times 10^{-7} \text{ cm}^2/\text{s}$ at $51 \text{ }^\circ\text{C}$ (Scheidt et al., 2005) are fairly close to $0.95 \times 10^{-7} \text{ cm}^2/\text{s}$ obtained from simulation for the 288 system, but differ greatly from the $2.92 \times 10^{-7} \text{ cm}^2/\text{s}$ from the 72 lipid system (Klauda et al., 2006a). The short-time diffusion constant, sometimes denoted, D_ℓ^{cage} , is obtained from neutron scattering, and equals $12.0 \times 10^{-7} \text{ cm}^2/\text{s}$ at $55 \text{ }^\circ\text{C}$ (Tabony and Perly, 1991). The simulated values, 13.9 and $14.7 \times 10^{-7} \text{ cm}^2/\text{s}$ for the large and the small systems, respectively, agree well with this value.

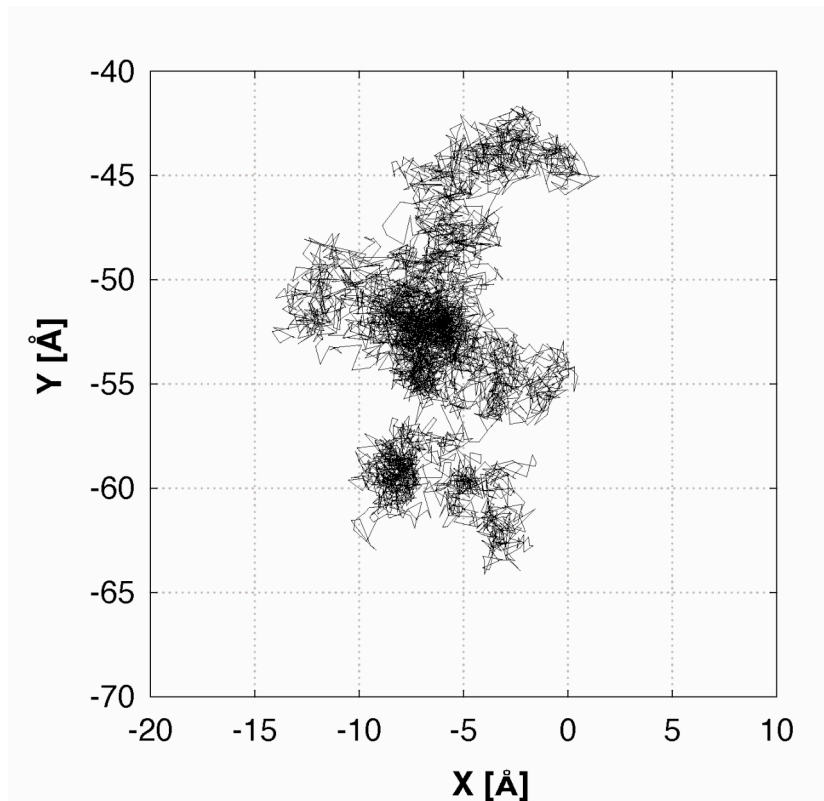


Figure 13. The lateral trace (in 10-ps intervals) of the center of mass of a lipid over 50 ns in the simulation of 288 lipids (Klauda et al., 2006a).

The difference in D_ℓ for the two systems is a striking example of a finite size artifact. This is analyzed in detail using a Poisson analysis based on clusters calculated from the CM trajectory (Klauda et al., 2006a), but a qualitative explanation gets to the core of the effect. Each leaflet in the 72 lipid system is a periodic 6 x 6 array of lipids. A jump of one perturbs its neighbors and propagates across the periodic boundaries leading to bursts of highly correlated transitions. In contrast, the disturbance associated with a jump dissipates before the periodicity of the 288 lipid system comes into play. Removing the net displacement of each leaflet substantially lowers the apparent diffusion constant of the smaller system, but only hides the artifact and is therefore not appropriate. A more general lesson is: if an effect seems especially interesting, confirm it's not an artifact. In this case, quadrupling the size of the system was well worth it.

As a final point, a jump model affords estimates that set the time scale of the diffusion process and, thereby, the statistical errors in the simulation. The diffusion constant is related to the jump rate λ by

$$D_\ell = \frac{\lambda b^2}{4} \quad (20)$$

where b is the jump length (7.5 Å from the analysis in Klauda et al. (2006a)). Rounding to one significant figure, $\lambda = 4 \times (1 \times 10^{-7}) / (8 \times 10^{-8}) = 0.06 \times 10^9 \text{ s}^{-1}$. This yields 3 transitions per lipid in the 50 ns simulation (one jump every 15 ns), and approximately $N = 900$ total transitions for 288 lipid system. From Poisson statistics, the statistical error in N , and therefore D_ℓ , is $N^{-1/2} = 1/30$, or 3%.

E. Elastic Moduli and Slow Averaging

The malleability of surface area of lipids is vital to their function in cells, so the elastic moduli of bilayers are an important target for parameterization. The bulk elastic modulus K_b is the inverse of the isothermal compressibility (Section II.C.3). The surface area elastic modulus, K_a , can be evaluated from derivatives or from fluctuations, as follows

$$K_a = A \left(\frac{d\gamma}{dA} \right)_T = \frac{k_B T \langle A_{tot} \rangle}{\langle \delta A_{tot}^2 \rangle} \quad (21)$$

where $\langle V \rangle$, $\langle A_{tot} \rangle$, $\langle \delta V^2 \rangle$ and $\langle \delta A_{tot}^2 \rangle$ are the average (total) volumes and areas, and their fluctuations. K_a has been measured for a range of phosphatidylcholines (Rawicz et al., 2000). After correcting surface fluctuations associated with undulations, the experimental values of K_a are all about 240 ± 15 dyn/cm. Hence, while K_a does not provide a sensitive measure for distinguishing phosphatidylcholines, it does provide a robust value for parameterization. The surface area compressibility is very sensitive to other components, including alcohols (Ly and Longo, 2004) and cholesterol (Evans and Rawicz, 1990). There does not appear to be many measurements of the bulk compressibility. The value for DPPC (Mitaku et al., 1978), 2.1×10^{10} dyn/cm², is comparable to incompressible fluids; *e.g.*, K_b for water (20 °C) and pentadecane (39 °C) are 2.2 and 1.1×10^{10} dyn/cm², respectively.

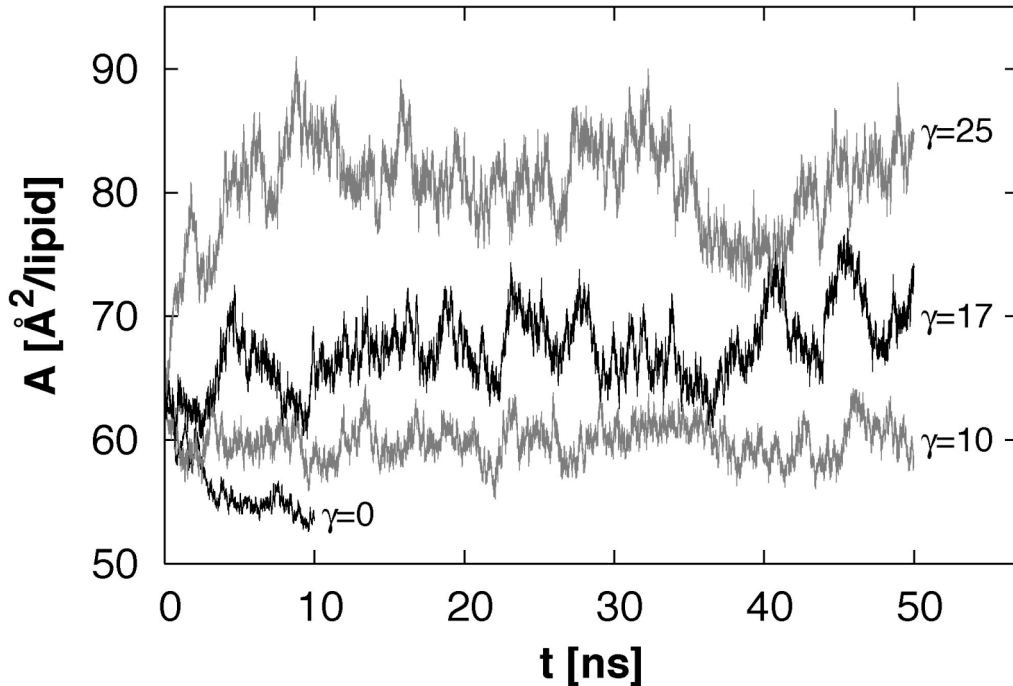


Figure 14. $NP\gamma T$ trajectories of DPPC carried out at 4 different applied surface tensions, including $\gamma=0$ (Venable et al., 2006).

It is useful to discuss two technical points before proceeding to the results of the calculations. First, the statistical errors in compressibilities of bilayers are large. Figure 14 plots the time series of a 50-ns trajectory of DPPC carried out at constant surface

tension $\gamma=17$ dyn/cm, PME for electrostatics, and a cutoff of 10 \AA for the LJ interactions. (These simulations were carried out before the introduction of the IPS method for LJ terms in CHARMM.) In spite of large fluctuations, the average surface area can be obtained with a 1% statistical error for a trajectory of this length. However, the statistical error in the *fluctuations* of a quantity is always higher than that of the quantity.

Consequently, the error in K_a is dominated by errors in $\langle \delta A_{tot}^2 \rangle$, leading to $K_a = 92 \pm 25$ dyn/cm. Similar considerations explain the large statistical error in the volume compressibility, $K_b = 1.5 \pm 0.4 \times 10^{10}$ dyn/cm².

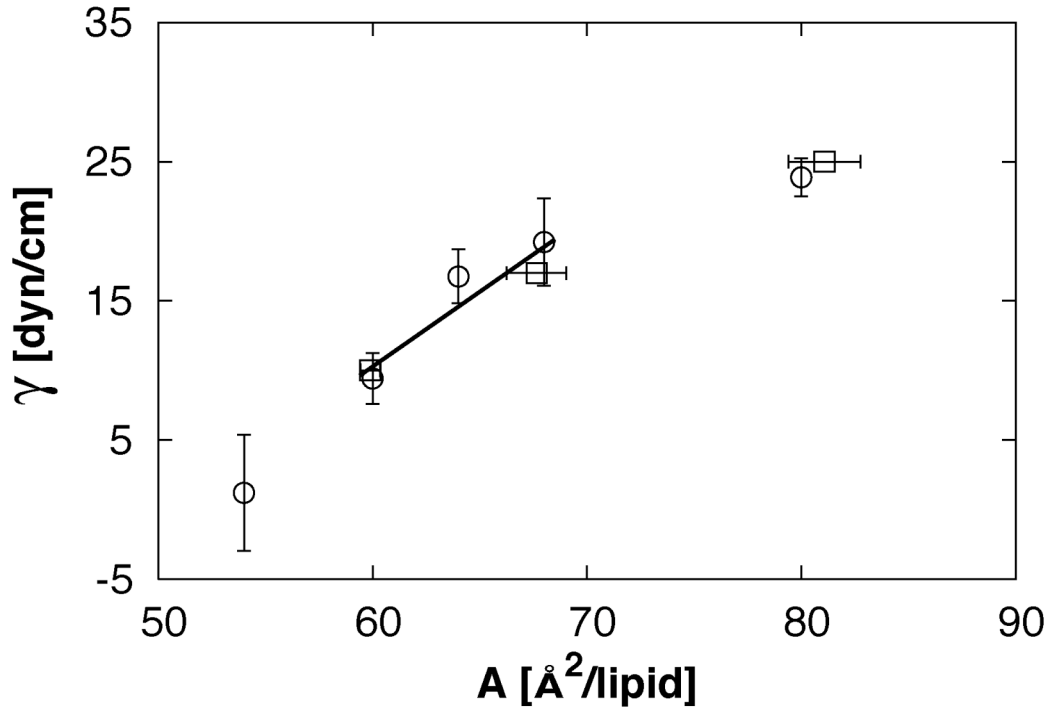


Figure 15. Surface tension-surface area isotherm for DPPC simulated at $NPAT$ (circles) and $NP\gamma T$ (squares). The solid line between 60 and shows the surface area range used to calculate the compressibility from $d\gamma/dA$ at $A=64 \text{ \AA}^2/\text{lipid}$ (Venable et al., 2006).

The second technical point is that K_a can also be evaluated from the derivative relation in Eq. (21). Because the $NPAT$ and $NP\gamma T$ ensembles yield statistically equivalent γ - A isotherms (Fig. 15), this allows some pooling of simulations at different surface area and surface tensions, and interpolation to areas not explicitly simulated. However, care

must be exercised to only use the linear regime of the γ - A isotherm. Figure 15 shows the γ - A isotherm for a combination of $NPAT$ and $NP\gamma T$ simulations of DPPC. Fitting the points between 59 and 68 $\text{\AA}^2/\text{lipid}$ (a total of 175 ns of data) yields $K_a = 138 \pm 26$ dyn/cm for $A=64$ $\text{\AA}^2/\text{lipid}$.

The simulated results for K_b and K_a underestimate experiment by over 30%. It is likely that a substantial portion of this error arises from the neglect of long-range LJ terms. Two results suggest this possibility. As already noted in Section II.C.3, addition of a long-range correction improves agreement of simulation and experiment for neat alkanes. While K_b for bilayers is most appropriately evaluated from $NP\gamma T$ simulations, volume fluctuations from recent from $NPAT$ simulations with a pressure-based LRC and with IPS yield 1.8 and 1.7×10^{10} dyn/cm², respectively; *i.e.*, approximately halfway between the values of 1.5 and 2.1×10^{10} dyn/cm² obtained by simulations with no long-range LJ and experiment. In summary, long-range Lennard-Jones terms should not be ignored when evaluating elastic constants.

F. Surface area in bilayers, and the value of the surface tension

A particularly thorny aspect of force field development is the surface area per lipid. This is partly because the quantity is difficult to obtain experimentally, and accurate values are only available for only a few single component bilayers (Nagle and Tristram-Nagle, 2000; Wiener et al., 1991). Hence there are few targets for calibration of parameters. To proceed further requires a discussion of the surface tension of a bilayer and a very delicate balance of forces.

C27r yields a surface tension of approximately 20 dyn/cm/side for a DPPC bilayer consisting of 72 lipids when simulated at the experimental surface area. The values for other phosphatidylcholines are comparable ((Klauda et al., 2006b), and unpublished data). In contrast, the experimental surface tension of pure black lipid films is only 1 dyn/cm (Tien and Diana, 1968). Furthermore, based on arguments regarding the balance of forces in self assembled systems (Israelachvili et al., 1977; Jahnig, 1996), the surface tension of a large flaccid vesicle is zero.

There are two different physical arguments that lead, in principle, to small or zero γ for a macroscopic sized bilayer. The first is sketched in Fig. 16. The tangential pressure in the head group/water interface is negative, as would be expected for an interface of water and an organic liquid. This negative pressure is balanced by a *positive* tangential pressure in the bilayer midplane arising from repulsive interactions of the chains. Integrating across the entire bilayer then leads to a net surface tension of zero at all length scales, even a microscopic patch. If this argument is correct, C27r is clearly flawed.

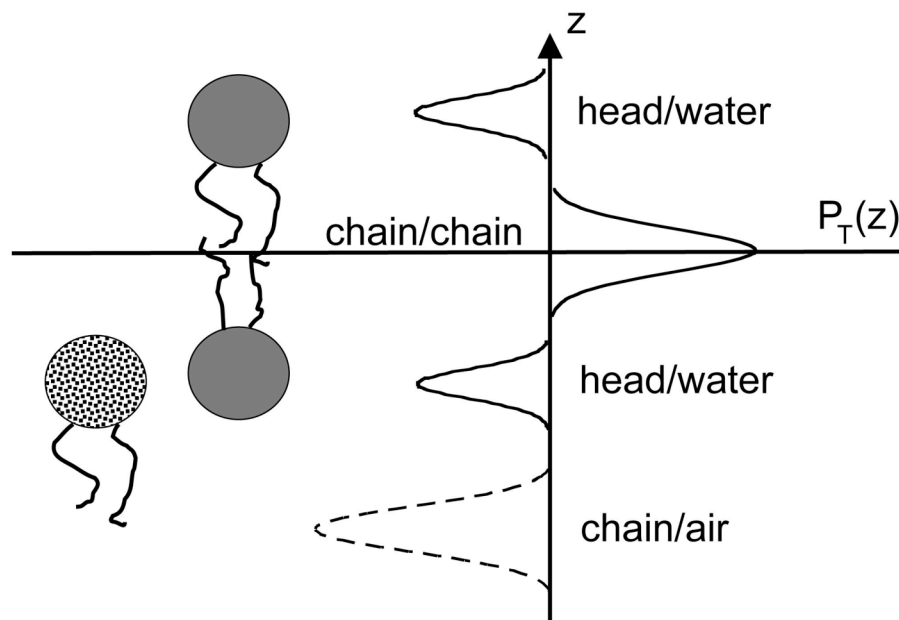


Figure 16. A schematic of the tangential profiles for a lipid bilayer (heads represented with grey circles) and a monolayer (stippled head).

The other explanation invokes the large undulations over thousands of angstroms that are known to occur in flaccid bilayers (Brochard et al., 1976). These entropic fluctuations balance the positive surface tension in small patches, and, on a *macroscopic* length scale, lead to a surface tension of near zero. In this view, the tangential pressure in the bilayer midplane could be positive, but not sufficiently positive to balance the negative tangential pressure in the head group/water interface. Estimates of the finite size

effect for simulation-sized patches vary. Initial estimates (Feller and Pastor, 1996) yielded the range 20-50 dyn/cm, which is comparable to the values obtained from simulation with C27r. A more rigorous analytical approach (Marsh, 1997) led to 4-6 dyn/cm. Pipette aspiration experiments (Rawicz et al., 2000) indicate that the tension required to smooth out a flaccid bilayer is less than a dyn/cm. Recent simulations based on the CHARMM potential on up to 288 (Castro-Roman et al., 2006) and 256 (Herce and Garcia, 2006) lipids have *not* shown evidence of system-size dependent surface tension. While much larger systems will be required to conclusively disprove the finite-size hypothesis, most evidence indicates that surface tensions obtained with C27r are too large.

One's view of the appropriate local surface tension, necessarily zero or potentially positive, impacts the process of parameterization. In the former, the requirement for zero surface tension can be (and perhaps should be) imposed. As an example, Berger et al., (1997), when developing an early version of a lipid FF used in many GROMOS based simulations, found that their original parameters yielded a positive surface tension, and then reduced the charges of head groups to yield zero surface tension. Sonne et al., (2007) have recently reparameterized the partial charges of the CHARMM C27r FF to obtain zero surface tension of DPPC near the experimental surface area. We have adopted the view that the surface tensions *could* be positive in a microscopic patch of membrane, and have therefore not imposed zero surface tension as a constraint. This is based on the notion that the realistic surface tension should arise from proper treatment of fundamental terms in the FF, and the realization that more than one variation of the parameters can yield zero surface tension. Nevertheless, surface tensions are routinely evaluated in the development process even though they are not used as a specific target.

Theoretical considerations aside, simulations of most bilayers using C27r must either be carried out at the experimental surface area in the *NPAT* ensemble or at *NP γ T* with an applied surface tension of approximately 20 dyn/cm to obtain sensible results. Most of our simulations related to parameterization are carried out at *NPAT*. Although the surface tension/surface area isotherms for *NPAT* and *NP γ T* are equivalent (Fig. 15), it is difficult to pick the precise value of the surface tension that yields the experimental area. However, simulating at *NPT* (equivalent to $\gamma=0$) leads to disaster: the surface

contracts from $64 \text{ \AA}^2/\text{lipid}$ to $52 \text{ \AA}^2/\text{lipid}$ (a gel-like state) in approximately 10 ns (Fig. 14). This because the “pulling in” of the surface tension of the system is not opposed by an applied surface tension. The same considerations apply to the GROMOS96 45A3 (Chandrasekhar et al., 2003) and General Amber Force Field (GAFF) (Joart and Martinek, 2007). Both show positive surface tensions at the experimental lipid surface area.

While there is arguably some uncertainty in the surface tension of a microscopic patch of a bilayer, the situation with monolayers is quite clear. Therefore, monolayers are an excellent target for parameterization. Figure 17 compares the γ - A isotherms for DPPC monolayers from simulation with C27r and experiment. The agreement is remarkably good, and indicates that the CHARMM FF captures the many interactions of lipid/water and alkane/air interfaces. Other parameter sets, including those explicitly tuned to yield zero surface tension for bilayers should be tested against monolayers.

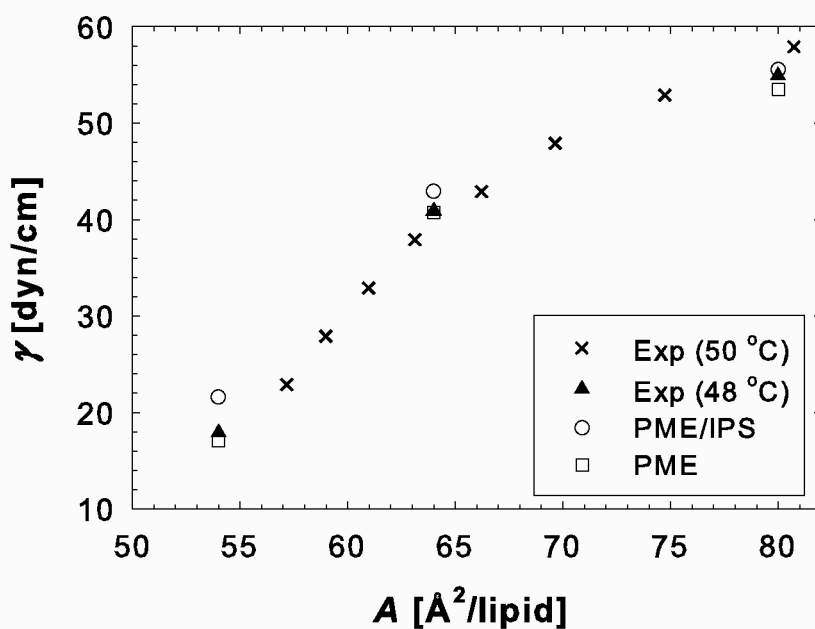


Figure 17. The simulated DPPC lipid monolayer surface tension at three surface areas for PME/IPS and PME with an $r_c=10 \text{ \AA}$ (Klauda et al., 2007). The experimental surface tensions, shown for 50 °C (Crane et al., 1999) and 48 °C (Somerharju et al., 1985) were obtained from Π/A isotherms using the relation $\Pi = \gamma_0 - \gamma$, where γ_0 is the surface tension of pure water at the experimental temperature.

The large positive surface tensions of monolayers, approximately 40 dyn/cm for DPPC at 64 Å²/lipid are consistent with both zero or positive surface tension for bilayers. In monolayers the chain/chain region is replaced by the chain/air interface. The tangential pressure profile thus contains two regions of negative pressure, as sketched in Fig. 16. Because the monolayer is macroscopically flat, there is no cancellation by undulations. If the surface tension of the chain/air interface is assumed to be equal to that of hexadecane/air (25 dyn/cm), the head group/water surface tension of a monolayer is about 15 dyn/cm. This value is close to the bilayer surface tensions presently obtained with C27r.

As a final technical point, the *NPT* simulation described above was carried out in tetragonal boundary conditions (the surface area and height can respond independently). A bilayer simulated in cubic conditions, where the shape of the cell is preserved, will not shrink substantially when simulated at *NPT*. This is because the pressure increases upon even a small volume contraction prevent further decrease in either height or surface area.

G. Dipole potentials and polarizable force fields

The dipole potential in a neutral membrane arises from the nonuniform distribution charges normal to interface. Given the importance of electrostatic signaling by molecules including phosphoinositides such as PIP2 and PIP3, the dipole potential is a natural target for a FF. Unfortunately, the absolute dipole potential is not possible to obtain for simple interfaces such as water/air (Paluch, 2000) or alkane/air, and values do not seem to be available for alkane/water interfaces. Hence, unlike the surface tension, simple systems do not provide undisputable target data. Furthermore, the dipole potential of bilayers is difficult to measure, and many results are considered controversial because of localization of voltage sensitive dyes. The range 225-250 mV is considered reasonable (Clarke, 2001), although recent experiments based on freeze-fracture raise the possibility that the true value is higher (Wang et al., 2006).

The dipole potential is calculated from a simulation by double integration of the Poisson's equation,

$$\psi(z) - \psi(0) = -\frac{4\pi}{\epsilon_0} \int_0^\infty \int_z^\infty \rho_c(z'') dz'' dz' \quad (22)$$

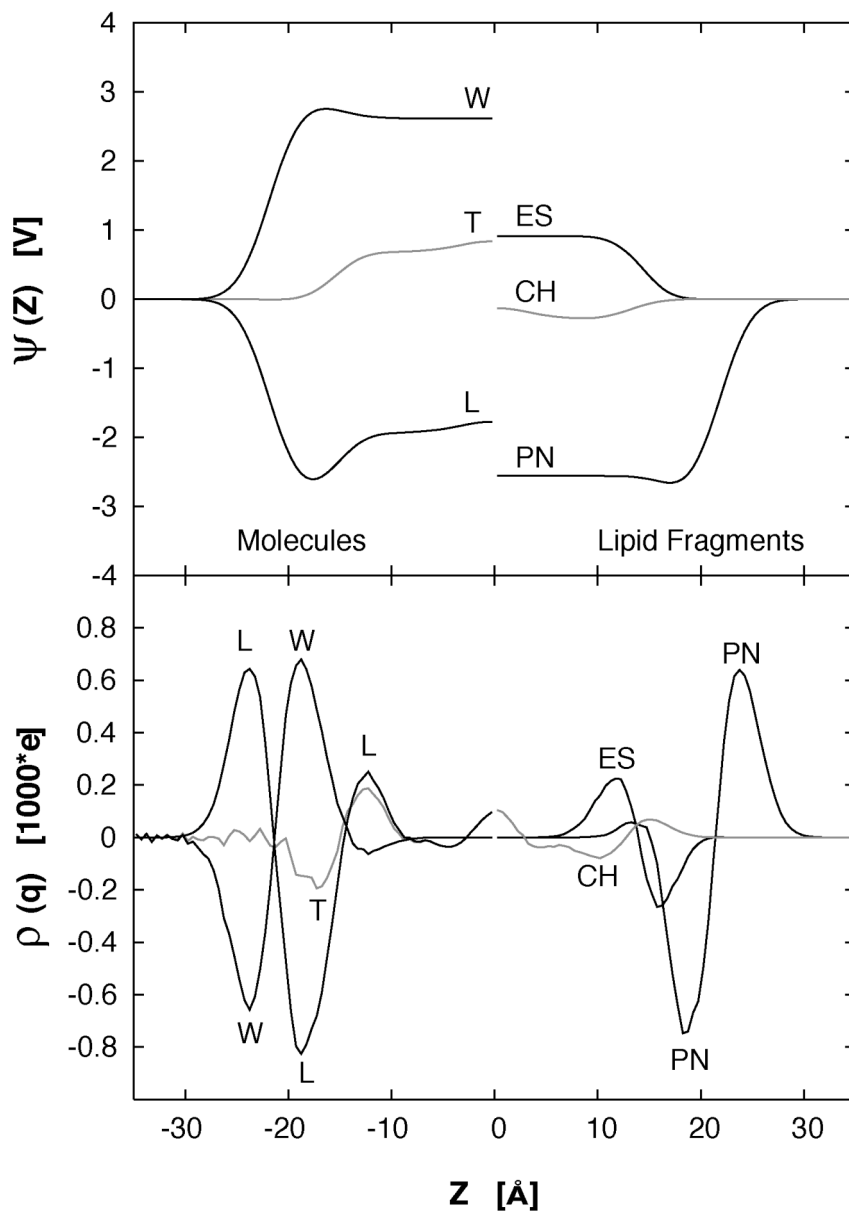


Figure 18. The simulated dipole potential of DPPC for the lipids (L), water (W) and total (T) (top left), and the acyl chains (CH), ester (ES) and PN groups (top right). CH includes carbons 2-16 of each chain; ES contains the glycerol C_{G1} and C_{G2} , C_1 of each chain and all atoms between; PN includes C_{G3} and phosphocholine group. The fragments are electrically neutral, and include bound hydrogens. The bottom plots the charge distribution for each of the preceding entities.

where ρ_c is the time averaged charge density. The results are shown in the top panel of Fig. 18. Starting with the left side, the total potential drop proceeds from the center of the bilayer ($z=0$) to the center of the water ($z=-33$). The value is 0.850 V, well over 3 times

that of experiment. This impressive level of disagreement can be seen as the sum of two much larger terms: a 2.7 V drop for the water, and a 1.9 V rise for the lipid. The right hand side of the plot shows the contributions of the chains, the ester and PN groups. The PN group dominates, while the chains contribute relatively little, as expected from the small partial charges on the carbons and hydrogens. The potential drop associated with the ester group approximately equals that of the entire system. Further insight is obtained from the charge component charge distributions. While the large (and mostly compensating) values in the head group/water interface are not surprising, the excess positive charge in the center the bilayer is a possible cause for concern and will be monitored in future development.

It is clear from Fig. 18 that better agreement with experiment could be obtained in a variety of ways; *e.g.*, increasing the magnitude of the PN contributions or decreasing that of the water. However, as noted in Section II, the charges on these components were developed in part by fitting to solvation data. Studies of polarizable models have shown that the charges and dipoles of additive modes tend to be too large, a consequence of correctly obtaining the free energies of solvation. Charges in polarizable models are smaller, and dipole potentials of simple systems are substantially smaller (Patel and Brooks, 2006; Vorobyov et al., 2007). It is possible that the correct description of the dipole potential drop in membranes will require an explicit treatment of polarizability.

Summary and Perspectives

This chapter contains two broad themes. The first is the underlying approach to development of the CHARMM force field. This begins with *ab initio* calculations of small molecules, adjustments as necessary to reproduce target data of condensed phases of these and closely related molecules, and special attention to the balance of solute-solute, solvent-solvent, and solute-solvent interactions. After the small molecule results are satisfactory, the potential function suitable for simulation of the large assembly (in this case a lipid bilayer) is formulated, and simulations are carried out to compare with appropriate target data. It is not likely that the basic approach will change in the near future, because it provides a fundamental connection to the underlying physics of the system.

The second theme of this chapter is the applicable *ab initio* and molecular dynamics methods, and the targets for validation. These change continually, and sometimes rapidly. Advances in methodology and increases computer speed and memory will permit *ab initio* calculations at higher levels of theory, more complete basis sets for larger systems, and explicit treatment of condensed phases. Molecular dynamics trajectories will be longer and on larger assemblies. Additional high-quality experimental data on lipid systems, including mixtures, will become available. Even the form of the potential energy function, Eq. (1), will change as more complex interactions (*e.g.*, polarizability) can be treated efficiently. In this sense, the chapter describes a “snapshot” of the force field, and its development and validation.

So, how good is the CHARMM lipid force field? This is actually two questions. The first regards the comparison with the experimental target data. The second pertains what can be accomplished by a simulation using the force field. The following paragraphs consider both.

A simulation focusing on the bilayer interior can be carried out with high confidence. This is because the densities, isothermal compressibilities, diffusivities, viscosities (Table 1), surface tensions (Table 2), and NMR T_1 's of medium length bulk alkanes (Fig. 5) are in virtually quantitative agreement with experiment. As discussed in Section III.B and illustrated in Fig. 9, the conformational distributions of alkanes and the acyl chains of bilayers are nearly identical for chains of the same length. The excellent agreement of simulation and experiment for the acyl chain deuterium order parameters (Fig. 8) follows, in part, from the careful parameterization of alkanes.

Density profiles for bilayers of DMPC and DPPC (Fig. 7) also agree well with x-ray diffraction data, and many features of the head group region are within 15-30% of experiment. These include the NMR T_1 's (Fig. 10), lateral diffusion constants (Fig. 12), the surface area elastic modulus (Fig. 15), and the surface pressure-surface area monolayer isotherm (Fig. 17). Hence, the FF provides the essential bilayer environment (hydrophobic interior/hydrophilic surface) necessary for the stability of membrane proteins. Less satisfactory are the deuterium order parameters of the glycerol-carbonyl region (Fig. 8), and the dipole potential drop (Fig. 18). These deficiencies potentially

limit studies concerned with detailed lipid protein interactions, and the interactions of ionic species with the head group/water interface.

CHARMM parameters for singly and polyunsaturated chains have been validated in a manner comparable to DPPC. Parameters for phosphatidylethanolamine and cholesterol are available, but have not been exhaustively tested. Sphingomyelin and glycolipids are under study. Hence, some biologically more relevant membranes can be simulated, though with somewhat less confidence than pure phosphatidylcholine bilayers. Because the surface areas of multicomponent bilayers are not well known, it is advisable to simulate at a range of surface areas in order to bracket the correct value. If the effect under consideration is very sensitive to the surface area, results of the simulation must be interpreted with extra caution.

Naturally, simulations must be carried out appropriately to obtain the mostly good agreement with experiment described in this chapter. In this chapter, the effects of long-range Lennard-Jones interactions, finite system size, and surface tension were highlighted. Long-range LJ interactions make substantial contributions to the densities, compressibilities (Section II.C.1), and surface tensions (Section II.C.2 and Table 2) of liquid alkanes. Bilayers are more than half alkane, and should be simulated with the isotropic periodic sum method, the pressure-based long-range correction, or a very long cutoff. Translational diffusion is sensitive to finite size effects in both neat fluids and bilayers, though the origins of the effects appear to be different. Equation (6) indicated that the alkane diffusion constants calculated directly with the simulation were increased 25% by the finite size correction (Table 1). In contrast, the lateral diffusion constant of DPPC decreased by more than a factor of three when the system size increased from 72 to 288 lipids (Fig. 12). With this notable exception, systems of 72 lipids are adequate for evaluation the targets described in Section III. This does not imply that larger systems are not important for parameter testing. The simulation of large systems will probe collective motions accessible by NMR relaxation times obtained at lower frequencies (< 15 MHz), and lend insight into role of undulations. The most controversial aspect of the CHARMM lipid FF is the presence of a positive surface tension for DPPC at its experimental surface area. From a purely practical point of view, simulations must be carried out at constant surface area (NVT or $NPAT$) or constant surface tension ($NP\gamma T$);

the two ensembles are equivalent (Fig. 15). The latter is recommended when it is necessary to include area fluctuations, such as when simulating peptide insertion. Simulating at $NP\gamma T$ is no more difficult than simulating NPT , and the surface area will be maintained (Fig. 14). Simulating complex systems at several different applied surface tensions is recommended.

Present force field development efforts for DPPC are focused on the glycerol-carbonyl region. Resolving the discrepancy of calculated and experimental deuterium order parameters (Fig. 8) at carbon 2 of the chains and carbon 1 of the glycerol is the highest priority. A change in structure of this region would modulate the dipole potential, which is the sum of large negative and positive contributions (Fig. 16). Correctly describing the inequivalence of the chains near the head group should also shift the methyl and methylene distributions in the bilayer center (Fig. 7). Specifically, offsetting chain 2 slightly closer to the lipid/water interface than chain 1 would reduce the methylene density and increase the methyl density and thereby improve agreement with experiment. The effect on the surface tension is less clear, given that surface tensions of monolayers agree well with experiment (Fig. 17). Nevertheless, the bilayer surface tension includes contributions from both the surface and the interior (Fig. 16), so some changes are expected.

A polarizable lipid force field is a longer term goal. The results of simulations with such a FF will provide insight into some of the discrepancies with experiment discussed here, notably the dipole potential, and may prove essential for simulating membranes with charged lipids and ions. Proceeding to more detail, combined quantum mechanics/molecular mechanics (QM/MM) will be required to simulate chemical reactions in membranes. At the other extreme, coarse grained models allow simulations of huge patches of membranes and thereby can be used to study fusion, mixed phases, and raft formation. Reliable potentials will be required in each case. The basic approach outline in this chapter will allow their development.

Acknowledgments

This work has profited from many valuable interactions with both experimentalists and theorists. We especially thank Bernard Brooks, Michael Brown, Scott Feller, Klaus Gawrisch, Adrian Parsegian, John Nagle, Attila Szabo, Douglas Tobias and Steven White. This research was supported in part by the Intramural Research Program of the NIH, National Heart, Lung and Blood Institute. Some of the simulation results presented here utilized the high-performance computational capabilities of the Biowulf PC/Linux cluster at the National Institutes of Health, Bethesda, MD. (<http://biowulf.nih.gov>) Financial support from the NIH (GM51501 and GM072558) and computational support from the DOD ASC Major Shared Resource Computing and PSC Pittsburgh Supercomputing Center to ADM Jr. are acknowledged

References

- Allen, M. P., and Tildesley, D. J. (1987). *Computer Simulations of Liquids*. Clarendon Press, Oxford.
- Bayly, C. I., Cieplak, P., Cornell, W. D., and Kollman, P. A. (1993). *Journal of Physical Chemistry* **97**, 10269-10280.
- Becke, A. D. (1993). *Journal Of Chemical Physics* **98**, 5648-5652.
- Benz, R. W., Castro-Roman, F., Tobias, D. J., and White, S. H. (2005). *Biophysical Journal* **88**, 805-817.
- Berger, O., Edholm, O., and Jahnig, F. (1997). *Biophysical Journal* **72**, 2002-2013.
- Brochard, F., Degennes, P. G., and Pfeuty, P. (1976). *Journal De Physique* **37**, 1099-1104.
- Brooks, B. R., Bruccoleri, R. E., Olafson, B. D., States, D. J., Swaminathan, S., and Karplus, M. (1983). *Journal of Computational Chemistry* **4**, 187-217.
- Brown, M. F., Ribeiro, A. A., and Williams, G. D. (1983). *Proceedings of the National Academy of Sciences of the United States of America-Biological Sciences* **80**, 4325-4329.
- Brown, M. F., Thurmond, R. L., Dodd, S. W., Otten, D., and Beyer, K. (2002). *Journal of the American Chemical Society* **124**, 8471-8484.
- Brown, M. L., Venable, R. M., and Pastor, R. W. (1995). *Biopolymers* **35**, 31-46.
- Buck, M., Bouguet-Bonnet, S., Pastor, R. W., and MacKerell, A. D. (2006). *Biophysical Journal* **90**, L36-L38.
- Buldt, G., Gally, H. U., Seelig, J., and Zaccai, G. (1979). *Journal of Molecular Biology* **134**, 673-691.

- Bush, B. L., Bayly, C. I., and Halgren, T. A. (1999). *Journal Of Computational Chemistry* **20**, 1495-1516.
- Cances, E., Mennucci, B., and Tomasi, J. (1997). *Journal Of Chemical Physics* **107**, 3032-3041.
- Castro-Roman, F., Benz, R. W., White, S. H., and Tobias, D. J. (2006). *Journal of Physical Chemistry B* **110**, 24157-24164.
- Chandrasekhar, I., Kastenholz, M., Lins, R. D., Oostenbrink, C., Schuler, L. D., Tieleman, D. P., and van Gunsteren, W. F. (2003). *European Biophysics Journal with Biophysics Letters* **32**, 67-77.
- Chen, I. J., Yin, D. X., and MacKerell, A. D. (2002). *Journal Of Computational Chemistry* **23**, 199-213.
- Chirlian, L. E., and Francl, M. M. (1987). *Journal Of Computational Chemistry* **8**, 894-905.
- Clarke, R. J. (2001). *Advances in Colloid and Interface Science* **89**, 263-281.
- Cossi, M., Scalmani, G., Rega, N., and Barone, V. (2002). *Journal Of Chemical Physics* **117**, 43-54.
- Crane, J. M., Putz, G., and Hall, S. B. (1999). *Biophysical Journal* **77**, 3134-3143.
- Curtiss, L. A., Raghavachari, K., Redfern, P. C., Rassolov, V., and Pople, J. A. (1998). *Journal of Chemical Physics* **109**, 7764-7776.
- Curtiss, L. A., Redfern, P. C., Raghavachari, K., Rassolov, V., and Pople, J. A. (1999). *Journal of Chemical Physics* **110**, 4703-4709.
- Darden, T., York, D., and Pedersen, L. (1993). *Journal of Chemical Physics* **98**, 10089-10092.
- Davis, J. H. (1983). *Biochimica Et Biophysica Acta* **737**, 117-171.
- Douglass, D. C., and McCall, D. W. (1958). *Journal of Physical Chemistry* **62**, 1102-1107.
- Duan, Y., Wu, C., Chowdhury, S., Lee, M. C., Xiong, G. M., Zhang, W., Yang, R., Cieplak, P., Luo, R., Lee, T., Caldwell, J., Wang, J. M., and Kollman, P. (2003). *Journal of Computational Chemistry* **24**, 1999-2012.
- Dunning, T. H. (2000). *Journal of Physical Chemistry A* **104**, 9062-9080.
- Dunning, T. H., Peterson, K. A., and Wilson, A. K. (2001). *Journal of Chemical Physics* **114**, 9244-9253.
- Ernzerhof, M., and Scuseria, G. E. (1999). *Journal of Chemical Physics* **110**, 5029-5036.
- Evans, E., and Rawicz, W. (1990). *Physical Review Letters* **64**, 2094-2097.
- Feig, M., MacKerell, A. D., Jr., and Brooks, C. L. (2003). *Journal of Physical Chemistry B* **107**, 2831-2836.
- Feller, S. E., and MacKerell, A. D., Jr. (2000). *Journal of Physical Chemistry B* **104**, 7510-7515.
- Feller, S. E., and Pastor, R. W. (1996). *Biophysical Journal* **71**, 1350-1355.
- Feller, S. E., Pastor, R. W., Rojnuckarin, A., Bogusz, S., and Brooks, B. R. (1996). *Journal of Physical Chemistry* **100**, 17011-17020.
- Feller, S. E., Venable, R. M., and Pastor, R. W. (1997a). *Langmuir* **13**, 6555-6561.
- Feller, S. E., Yin, D. X., Pastor, R. W., and MacKerell, A. D., Jr. (1997b). *Biophysical Journal* **73**, 2269-2279.
- Gally, H. U., Pluschke, G., Overath, P., and Seelig, J. (1981). *Biochemistry* **20**, 1826-1831.

- Gross, J. D., Warschawski, D. E., and Griffin, R. G. (1997). *Journal of the American Chemical Society* **119**, 796-802.
- Hauser, H., Pascher, I., and Sundell, S. (1980). *Journal of Molecular Biology* **137**, 249-264.
- Henchman, R. H., and Essex, J. W. (1999). *Journal Of Computational Chemistry* **20**, 483-498.
- Herce, H. D., and Garcia, A. E. (2006). *Journal of Chemical Physics* **125**.
- Holler, F., and Callis, J. B. (1989). *Journal of Physical Chemistry* **93**, 2053-2058.
- Horn, H. W., Swope, W. C., Pitera, J. W., Madura, J. D., Dick, T. J., Hura, G. L., and Head-Gordon, T. (2004). *Journal Of Chemical Physics* **120**, 9665-9678.
- Israelachvili, J. N., Mitchell, D. J., and Ninham, B. W. (1977). *Biochimica Et Biophysica Acta* **470**, 185-201.
- IUPAC. (1967). *Journal of Lipid research* **8**, 523-528.
- Jahnig, F. (1996). *Biophysical Journal* **71**, 1348-1349.
- Jakalian, A., Bush, B. L., Jack, D. B., and Bayly, C. I. (2000). *Journal Of Computational Chemistry* **21**, 132-146.
- Jojart, B., and Martinek, T. A. (2007). *Journal of Computational Chemistry* **in press**.
- Jorgensen, W. L. (1986). *Journal Of Physical Chemistry* **90**, 1276-1284.
- Jorgensen, W. L., Chandrasekhar, J., Madura, J. D., Impey, R. W., and Klein, M. L. (1983). *Journal of Chemical Physics* **79**, 926-935.
- Jorgensen, W. L., Madura, J. D., and Swenson, C. J. (1984). *Journal Of The American Chemical Society* **106**, 6638-6646.
- Jorgensen, W. L., Maxwell, D. S., and Tiradorives, J. (1996). *Journal of the American Chemical Society* **118**, 11225-11236.
- Karaborni, S., and O'Connell, J. P. (1990). *Journal of Chemical Physics* **92**, 6190-6194.
- Klauda, J. B., Brooks, B. R., MacKerell, A. D., Jr., Venable, R. M., and Pastor, R. W. (2005a). *Journal of Physical Chemistry B* **109**, 5300-5311.
- Klauda, J. B., Brooks, B. R., and Pastor, R. W. (2006a). *Journal of Chemical Physics* **125**, 144710
- Klauda, J. B., Garrison, S. L., Jiang, J., Arora, G., and Sandler, S. I. (2004). *Journal of Physical Chemistry A* **108**, 107-112.
- Klauda, J. B., Kučerka, N., Brooks, B. R., Pastor, R. W., and Nagle, J. F. (2006b). *Biophysical Journal* **90**, 2796-2807.
- Klauda, J. B., Pastor, R. W., and Brooks, B. R. (2005b). *Journal of Physical Chemistry B* **109**, 15684-15686.
- Klauda, J. B., Wu, X. W., Pastor, R. W., and Brooks, B. R. (2007). *Journal of Physical Chemistry B* **Accepted**.
- Kučerka, N., Tristram-Nagle, S., and Nagle, J. F. (2006). *Biophysical Journal* **90**, L83-L85.
- Lagüe, P., Pastor, R. W., and Brooks, B. R. (2004). *Journal of Physical Chemistry B* **108**, 363-368.
- Laio, A., VandeVondele, J., and Rothlisberger, U. (2002). *Journal Of Physical Chemistry B* **106**, 7300-7307.
- Lamoureux, G., MacKerell, A. D., and Roux, B. (2003). *Journal Of Chemical Physics* **119**, 5185-5197.

- Lemmon, E. W., McLinden, M. O., and Friend, D. G. (2005). Thermophysical Properties of Fluid Systems. In "NIST Chemistry WebBook, NIST Standard Reference Database Number 69" (P. J. Linstrom and W. G. Mallard, eds.). National Institute of Standards and Technology, Gaithersburg, MD.
- Levine, Y. K., and Wilkins, M. H. F. (1971). *Nature New Biology* **230**, 69-72.
- Lewis, B. A., and Engelman, D. M. (1983). *Journal of Molecular Biology* **166**, 211-217.
- Lide, D. R. (2000). CRC Handbook. CRC Press, Boca Raton, FL.
- Lipari, G., and Szabo, A. (1982). *Journal of the American Chemical Society* **104**, 4546-4559.
- Ly, H. V., and Longo, M. L. (2004). *Biophysical Journal* **87**, 1013-1033.
- Lyerla, J. R., Jr., McIntyre, H. M., and Torchia, D. A. (1974). *Macromolecules* **7**, 11-14.
- MacKerell, A. D. (2001). Atomistic Models and Force Fields. In "Computational Biochemistry and Biophysics" (O. M. Becker, A. D. MacKerell, B. Roux and M. Watanabe, eds.), pp. 7-38. Marcel Dekker, New York.
- MacKerell, A. D. (2004). *Journal of Computational Chemistry* **25**, 1584-1604.
- MacKerell, A. D. (2005). Interatomic Potentials: Molecules. In "Handbooks of Material Modeling" (S. Yip, ed.), pp. 509-525. Springer, Netherlands.
- MacKerell, A. D. (2007).
- MacKerell, A. D., Feig, M., and Brooks, C. L. (2004). *Journal of Computational Chemistry* **25**, 1400-1415.
- MacKerell, A. D., Jr., Bashford, D., Bellott, M., Dunbrack, R. L., Evanseck, J. D., Field, M. J., Fischer, S., Gao, J., Guo, H., Ha, S., Joseph-McCarthy, D., Kuchnir, L., Kuczera, K., Lau, F. T. K., Mattos, C., Michnick, S., Ngo, T., Nguyen, D. T., Prodhom, B., Reiher, W. E., Roux, B., Schlenkrich, M., Smith, J. C., Stote, R., Straub, J., Watanabe, M., Wiorkiewicz-Kuczera, J., Yin, D., and Karplus, M. (1998). *Journal of Physical Chemistry B* **102**, 3586-3616.
- MacKerell, A. D., and Karplus, M. (1991). *Journal Of Physical Chemistry* **95**, 10559-10560.
- MacKerell, A. D., Wiorkiewiczkuczera, J., and Karplus, M. (1995). *Journal Of The American Chemical Society* **117**, 11946-11975.
- Marsh, D. (1997). *Biophysical Journal* **73**, 865-869.
- Merz, K. M. (1992). *Journal Of Computational Chemistry* **13**, 749-767.
- Mitaku, S., Ikegami, A., and Sakanishi, A. (1978). *Biophysical Chemistry* **8**, 295-304.
- Nagle, J. F., and Tristram-Nagle, S. (2000). *Biochimica et Biophysica Acta-Reviews on Biomembranes* **1469**, 159-195.
- Oostenbrink, C., Villa, A., Mark, A. E., and Van Gunsteren, W. F. (2004). *Journal Of Computational Chemistry* **25**, 1656-1676.
- Ottiger, M., and Bax, A. (1998). *Journal of the American Chemical Society* **120**, 12334-12341.
- Paluch, M. (2000). *Advances in Colloid and Interface Science* **84**, 27-45.
- Pascher, I., Lundmark, M., Nyholm, P. G., and Sundell, S. (1992). *Biochimica Et Biophysica Acta* **1113**, 339-373.
- Pastor, R. W., Venable, R. M., and Feller, S. E. (2002). *Accounts of Chemical Research* **35**, 438-446.
- Patel, S., Mackerell, A. D., and Brooks, C. L. (2004). *Journal of Computational Chemistry* **25**, 1504-1514.

- Patel, S. A., and Brooks, C. L. (2006). *Journal of Chemical Physics* **124**.
- Raghavachari, K., Trucks, G. W., Pople, J. A., and Head-Gordon, M. (1989). *Chemical Physics Letters* **157**, 479-483.
- Rand, R. P., and Parsegian, V. A. (1989). *Biochimica Et Biophysica Acta* **988**, 351-376.
- Rawicz, W., Olbrich, K. C., McIntosh, T., Needham, D., and Evans, E. (2000). *Biophysical Journal* **79**, 328-339.
- Rick, S. W., and Stuart, S. J. (2002). Potentials and algorithms for incorporating polarizability in computer simulations. In "Reviews in Computational Chemistry, Vol 18", pp. 89-146.
- Roberts, M. F., and Redfield, A. G. (2004). *Journal of the American Chemical Society* **126**, 13765-13777.
- Scheidt, H. A., Huster, D., and Gawrisch, K. (2005). *Biophysical Journal* **89**, 2504-2512.
- Schlegel, H. B. (1982). *Journal of Computational Chemistry* **3**, 214-218.
- Schlenkrich, M., Brinkman, J., MacKerell, A. D., and Karplus, M. (1996). An Empirical Potential Energy Function for Phospholipids: Criteria for Parameter Optimization and Applications. In "Membrane Structure and Dynamics" (K. M. Merz and B. Roux, eds.), pp. 31-81. Birkhauser, Boston.
- Seelig, A., and Seelig, J. (1974). *Biochemistry* **13**, 4839-4845.
- Seelig, A., and Seelig, J. (1975). *Biochimica et Biophysica Acta* **406**, 1-5.
- Seelig, J. (1977). *Quarterly Reviews of Biophysics* **10**, 353-418.
- Seelig, J., Gally, H. U., and Wohlgemuth, R. (1977). *Biochimica Et Biophysica Acta* **467**, 109-119.
- Singh, U. C., and Kollman, P. A. (1984). *Journal Of Computational Chemistry* **5**, 129-145.
- Small, D. M. (1986). Handbook of Lipid Research. In "The Physical Chemistry of Lipids: From Alkanes to Phospholipids" (D. J. Hanahan, ed.). Plenum Press, New York.
- Somerharju, P. J., Virtanen, J. A., Eklund, K. K., Vainio, P., and Kinnunen, P. K. J. (1985). *Biochemistry* **24**, 2773-2781.
- Sonne, J., Jensen, M. O., Hansen, F. Y., Hemmingsen, L., and Peters, G. H. (2007). *Biophysical Journal* **in press**.
- Sundaralingam, M. (1972). *Annals of the New York Academy of Sciences USA* **195**, 324-355.
- Szabo, A. (1984). *Journal of Chemical Physics* **81**, 150-167.
- Szabo, A. (1986). *Ann. N.Y. Acad. Sci.* **482**, 44-50.
- Szabo, A., and Ostlund, N. S. (1996). Modern Quantum Chemistry: Introduction to Advanced Electronic Structure Theory. Dover Publication, Inc., Mineola.
- Tabony, J., and Perly, B. (1991). *Biochimica et Biophysica Acta* **1063**, 67-72.
- Tien, H. T., and Diana, A. L. (1968). *Chemistry and Physics of Lipids* **2**, 55-&.
- Vaz, W. L. C., Clegg, R. M., and Hallmann, D. (1985). *Biochemistry* **24**, 781-786.
- Venable, R. M., Brooks, B. R., and Pastor, R. W. (2000). *Journal of Chemical Physics* **112**, 4822-4832.
- Venable, R. M., Skibinsky, A., and Pastor, R. W. (2006). *Molecular Simulation* **In Press**.
- Vorobyov, I., Anisimov, V. M., Green, S., Venable, R. M., Moser, A., Pastor, R. W., and MacKerell, A. D. (2007). *Journal of Chemical Theory and Computation* **In Press**.
- Vorobyov, I. V., Anisimov, V. M., and MacKerell, A. D. (2005). *Journal of Physical Chemistry B* **109**, 18988-18999.

- Wang, J. M., Cieplak, P., and Kollman, P. A. (2000). *Journal of Computational Chemistry* **21**, 1049-1074.
- Wang, L. G., Bose, P. S., and Sigworth, F. J. (2006). *Proceedings of the National Academy of Sciences of the United States of America* **103**, 18528-18533.
- Warshel, A., and Lifson, S. (1970). *Journal Of Chemical Physics* **53**, 582-594.
- Wiener, M. C., King, G. I., and White, S. H. (1991). *Biophysical Journal* **60**, 568-576.
- Woodcock, H., Moran, D., Pastor, R. W., MacKerell, A. D., and Brooks, B. R. (2007). *Biophysical Journal* **Accepted**.
- Wu, X. W., and Brooks, B. R. (2005). *Journal of Chemical Physics* **122**, 044107.
- Yeh, I. C., and Hummer, G. (2004). *Journal of Physical Chemistry B* **108**, 15873-15879.
- Yin, D. X., and MacKerell, A. D. (1996). *Journal Of Physical Chemistry* **100**, 2588-2596.
- Yin, D. X., and MacKerell, A. D., Jr. (1998). *Journal of Computational Chemistry* **19**, 334-348.
- Zaccai, G., Buldt, G., Seelig, A., and Seelig, J. (1979). *Journal of Molecular Biology* **134**, 693-706.
- Zhang, Y. H., Feller, S. E., Brooks, B. R., and Pastor, R. W. (1995). *Journal of Chemical Physics* **103**, 10252-10266.
- Zhang, Y. H., Venable, R. M., and Pastor, R. W. (1996). *Journal of Physical Chemistry* **100**, 2652-2660.